The Impacts of Flood, Drought, and Turbidites on Organic Carbon Burial over the Past 2,000 years in the Santa Barbara Basin, California

Authors & Affiliations

Caitlyn T. Sarno[1*], Claudia R. Benitez-Nelson[1], Lori A. Ziolkowski[1], Ingrid L. Hendy[2], Catherine V. Davis[1], Eric J. Tappa[1], & Robert C. Thunell[1T]

[1] School of the Earth, Ocean & Environment, University of South Carolina, Columbia, SC, 29205 USA

[2] Department of Earth and Environmental Sciences, University of Michigan, Ann Arbor, MI, 48109 USA

[T] Deceased

*Corresponding Author: Caitlyn Sarno (caitsarno@gmail.com)

Key Points

- Terrestrial organic carbon is the dominant source of carbon to the SBB with deposition significantly increasing during flood events.
- Episodic flood and turbidite remobilization events were responsible for over 25% of the OC buried in the SBB over the past 2,000 years.
- Drought sedimentation had significantly lower sedimentation rates and had an *n*-alkane composition consistent with increased marine inputs.

This is the author manuscript accepted for publication and has undergone full peer review but has not been through the copyediting, typesetting, pagination and proofreading process, which may lead to differences between this version and the Version of Record. Please cite this article as doi: 10.1029/2020PA003849

Abstract

Climate conditions and instantaneous depositional events can influence the relative contribution of sediments from terrestrial and marine environments, and ultimately the quantity and composition of carbon buried in the sediment record. Here, we analyze the elemental, isotopic, and organic geochemical composition of marine sediments to identify terrestrial and marine sources in sediment horizons associated with droughts, turbidites, and floods in the Santa Barbara Basin (SBB), California during the last 2,000 years. Stable isotopes ($\delta^{13}C$ and $\delta^{15}N$), indicate that more terrestrial organic carbon (OC) was deposited during floods relative to background sediment, while bulk C to nitrogen (C/N) ratios remained relatively constant (~10). Long chain *n*-alkanes, (C_{27}, C_{29}, C_{31}, C_{33}), characteristic of terrestrial OC, dominated all types of sediment deposition, but were four times more abundant in flood layers. Marine algae (C_{15}, C_{17}, C_{19}) and macrophytes (C_{21}, C_{23}) were also two times higher in flood versus background sediments. Turbidites contained twice the terrestrial *n*-alkanes relative to background sediment. Conversely, drought intervals were only distinguishable from background sediment by their higher proportion of marine algal *n*-alkanes. Combined, our data indicate that 15% of the total OC buried in SBB over the past 2,000 years was deposited during 11 flood events where the sediment was mostly terrestrially derived, and another 12% of deep sediment OC burial was derived from shelf remobilization during 6 turbidite events. Relative to 20th century river runoff, our data suggests floods result in considerable terrestrial OC burial on the continental margins of California.

1. Introduction

Burial of organic carbon (OC) in marine sediments and coastal environments in particular, transfers carbon from the short term atmosphere-biosphere carbon cycle and into semi-permanent geological repositories. This carbon sequestration in the rock record ultimately influences global climate via the regulation of the greenhouse gas, carbon dioxide [*Berner*, 1982; *Martin et al*., 1987; *Sarmiento and Sundquist*, 1992; *Hedges and Keil*, 1995]. The quantity and composition of OC buried in marine sediments is controlled by its source and transport to the deep sea. Thus, understanding the sources of OC buried in marine sediments (e.g., terrestrial versus marine) provides insight into how coastal ecosystems influence carbon sequestration over geological time.

Oceanic primary productivity is hypothesized to account for 50% of the total global carbon fixed and approximately ten times the carbon annually produced by fossil fuel burning [*Smith and Hollibaugh*, 1993; *Schlesinger and Jiang*, 1991]. The coastal environment, while comprising a small proportion of the global oceans, plays a significant role in the carbon cycle due to its proximity to river runoff and nutrient rich waters that increase marine primary productivity [*Muller-Karger et al*., 2005; *Bianchi*, 2011]. Rivers carry significant terrestrial OC to the ocean, where it may be remineralized in the water column or buried in marine sediments [*Hedges and Keil*, 1995]. Small mountain river systems, such as those on the Southern California Margin, are an especially effective mechanism of OC burial. These systems are characterized by episodic discharge events and the sediments are more likely to survive coastal processing and reach the deep sea due to the characteristically narrow continental shelves of the margin [*Masiello and Druffel*, 2001]. Rapid sediment deposition events, such as turbidity currents (downslope remobilization of sediments) and floods, rapidly transport OC to low oxygen seafloor sediments where remineralization is less efficient, thus facilitating the burial of significant quantities of OC [*Burdige*, 2006].

Santa Barbara Basin (SBB), California is an optimal environment for paleoclimate reconstructions due to its suboxic bottom water and high sedimentation rate [*Soutar et al*., 1977; *Hendy et al*., 2013]. This creates an ideal location to examine the character and efficiency of carbon sequestration in a coastal environment. Here, we measured total OC (TOC), total nitrogen (TN), molar C/N ratios, $\delta^{13}C$ and $\delta^{15}N$ isotopes, and *n*-alkane biomarkers in a well-dated sediment core [*Hendy et al*., 2013] to elucidate the source of organic matter to marine sediments during episodic rapid deposition events (e.g., floods and turbidites) and lower sedimentation intervals (i.e., droughts). Understanding the composition of organic matter (OM) transported by different mechanisms and deposited under different environmental conditions provides information regarding how coastal ecosystems influence carbon sequestration over decadal to geologic timescales.

1.1 Study Site

Southern California often experiences floods and droughts due to its Mediterranean climate and in response to the El Niño Southern Oscillation (ENSO) and Pacific Decadal Oscillation (PDO) [*Soutar and Crill*, 1977; *Schimmelmann et al*., 2003; *Hendy et al*., 2015].

During the warm phases of ENSO and PDO, precipitation and river discharge increases, supplying more terrestrial sediment to the California coast [*Ropelewski and Halpert*, 1989; *Warrick and Farnsworth*, 2009; *Hendy et al.*, 2015]. In addition, these warm phases are associated with increased transport of warm, nutrient-depleted water from the subtropics, reducing marine productivity [*Chavez*, 1996; *Bograd and Lynn*, 2001]. The Western Coast of the United States is also vulnerable to extreme floods, termed megafloods [*Dettinger and Ingram*, 2013]. These megafloods are caused by excessive rain from atmospheric rivers that may be further enhanced by ENSO [*Dettinger and Ingram*, 2013]. Atmospheric rivers often occur on shorter time scales and are responsible for delivering 30-50% of the annual precipitation to California [*Dettinger and Ingram*, 2013].

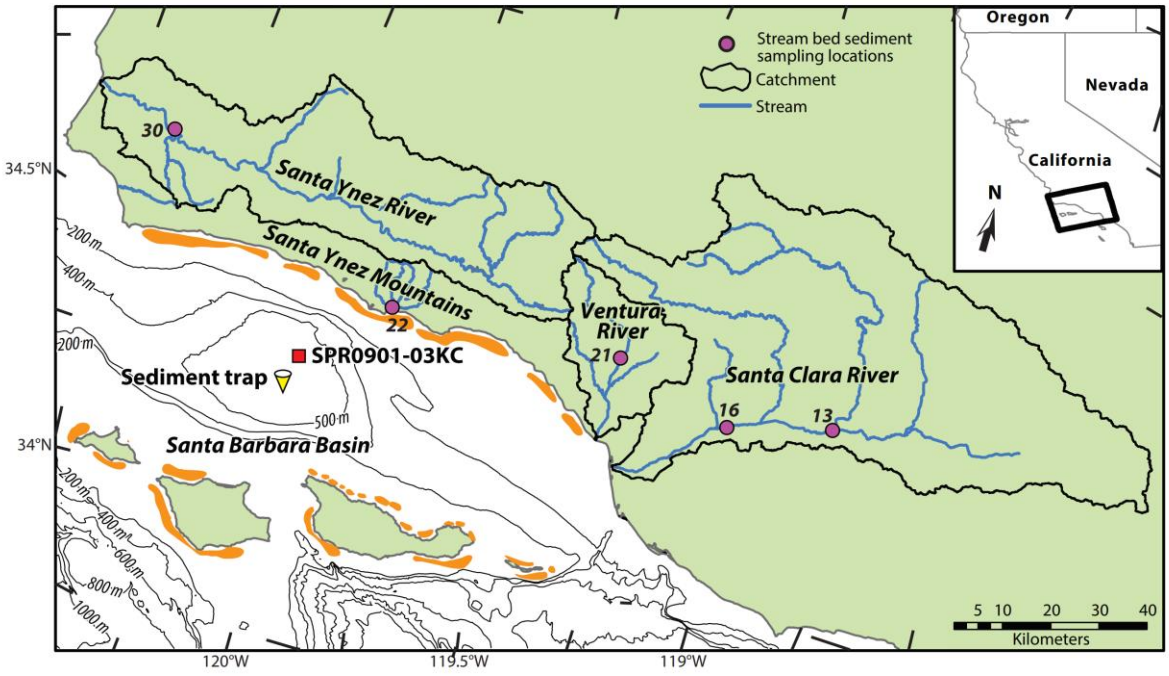

Figure 1: Map of the Santa Barbara Basin (SBB). The sediment core is labeled by the red square (34°16.99'N, 120°2.41'W), the sediment trap is denoted by the yellow triangle (34°14′N, 120°02′W), and the river collection sites are marked by the purple circles (see *Napier et al.* [2019]): Santa Clara River, location 13 (34˚23.10' N, 118˚47.22'W) and 16 (34˚20.70'N, 119˚01.46'W); Ventura River, location 21 (34˚25.20'N, 119˚ 17.94'W); and the Santa Ynez River, locations 22 (34˚24.60'N, 119˚49.74'W) and 30 (34˚38.40'N, 120˚24.54'W). Kelp beds are denoted by shaded orange regions in the nearshore environment of the SBB [*Schimmelmann and Tegner*, 1991].

The SBB is located off the coast of Southern California where it is bounded by mountains to the north, islands to the south, and sills to the east and west that impede circulation in the deep basin (Figure 1). Restricted circulation reduces the oxygen supply to bottom waters, creating a suboxic environment at a depth below 480 m [*Li et al*., 2009]. The resulting anoxic sediment minimizes bioturbation creating high resolution sedimentary records [*Hülsemann and Emery*, 1961; *Hendy et al*., 2013]. Highly refined age models have been developed for SBB sediments, thus there is an opportunity to examine episodic regional climate events, such as floods and droughts, over thousands of years [*Soutar et al*., 1977; *Schimmelmann et al*., 2003; *Hendy et al*., 2015].

Annually, there are two compositionally different periods of sedimentation in the SBB. During the winter, the North Pacific High and the Jet Stream migrate south, strengthening the Aleutian Low and causing mild, wet, and stormy conditions [*Dorman and Winant*, 2000; *Barron et al*., 2010]. These wet conditions increase terrestrial input via river discharge and sediment transport to the basin [*Hülsemann and Emery*, 1961; *Thunell et al*., 1995; *Hendy et al*., 2015]. During the spring/summer, the North Pacific High produces strong northerly winds that induce coastal upwelling in California and support high biological productivity [*Hülsemann and Emery*, 1961; *Thunell et al*., 1995; *Hendy et al*., 2013]. As a result marine biogenic sediment, dominated by diatoms (biogenic silica) and foraminifera (calcium carbonate), ultimately reach the basin bottom and are buried [*Barron et al*., 2010]. Biogenic sediment can enhance clay sedimentation by flocculation of clays onto marine snow [*Deuser et al*., 1983; *Thunell et al*., 1995]. Additional sources of sedimentary material in the spring/summer may include benthic bacterial mats (e.g., *Beggiatoa*) that form after winter terrestrial inputs [*Soutar and Crill*, 1977], or in response to annual oxygenation of the basin during upwelling periods [*Reimers et al*., 1990; *Bograd et al*., 2002]. Together, one terrestrial-rich and one biogenic-rich sediment lamina represent a single year [*Soutar and Crill*, 1977; *Thunell et al*., 1995; *Hendy et al*., 2015].

In addition to the annual lamina of terrestrial and marine sediment, this core also contained lamina consistent with floods, droughts, and turbidites. ENSO and PDO change precipitation patterns that produce floods (warm phase) and droughts (cold phase) in the SBB region [*Chavez*, 1996; *Schimmelmann et al*., 2003; *Graham et al*., 2007]. During a flood event, there is rapid transport of lithogenic sediment to the basin and annual laminae are replaced by a

thick, gray flood layer [*Barron et al*., 2015]. Turbidites are also present, distinctive from flood layers in that they transport sediment from the shelf into the deeper basin [*Du et al*., 2018]. Turbidites are visually distinct from flood deposits as they are characterized by an olive coloration and larger grain size [*Schimmelmann et al*., 1998; *Hendy et al*., 2013].

1.2 Geochemical Tools

The impacts of episodic flooding, turbidite events, and prolonged drought on carbon burial in the SBB are poorly understood. This study utilizes stable isotopes ($\delta^{13}C$, $\delta^{15}N$) of bulk sediments, TOC and TN concentrations, and *n*-alkane lipid biomarker concentrations to determine sediment composition from flood and turbidite events, drought periods, and background sediment. Background sediments were selected based on the absence of properties characteristic of floods, turbidites, or droughts. Carbon to nitrogen (C/N) ratios provide a broad view of organic matter (OM) source, where C/N molar ratios > 20 are indicative of the structural material required by land plants [*Hedges et al*., 1986]. However, C/N ratios are often imprecise due to the mixing of multiple sediment inputs (rivers, marine algae, vascular plants, etc.). As such, OM stable isotopes are also used to determine sediment source. In terrestrial environments, the isotopic composition of plants is usually depleted in the heavier isotopes (i.e., $\delta^{13}C_{terrestrial}$= -27‰ and $\delta^{15}N_{terrestrial}$ = 2‰), while marine sources tend to have a higher isotopic signal ($\delta^{13}C_{marine}$= -20‰ and $\delta^{15}N_{marine}$ = 10‰) [*Sweeney and Kaplan*, 1980; *Meyers*, 1994].

While C and N isotopes may distinguish OM source (marine versus terrestrial), these isotopes also undergo additional fractionation processes both in the water column and on land. Surface water entering SBB during the summer and fall flows northward from the Eastern Tropical North Pacific [*Bray et al*., 1999] where denitrification results in higher $\delta^{15}N$ by utilizing nitrate as a terminal electron acceptor in respiration in place of oxygen [*Emmer and Thunell*, 2000; *Voss et al*., 2001; *Brandes et al*., 2003; *Sigman et al*., 2003; *Davis et al*., 2019]. Denitrification raises the $\delta^{15}N$ signal as the lighter nitrogen isotope is preferentially utilized to form nitrogen gas, leaving behind an enriched pool of nitrogen [*Cline and Kaplan*, 1975]. It should be noted that additional denitrification sometimes occurs within the suboxic waters and anoxic sediments of the SBB [*Sigman et al*., 2003; *Thunell*, 2003]. In spring, strong winds stimulate upwelling of nutrient enriched waters, potentially resulting in sinking OM lower in $\delta^{15}N$ as organisms preferentially utilize the lighter isotopes of N in nitrate. This leaves the

remaining water enriched in ^{15}N until complete nitrate utilization occurs [*Davis et al*., 2019]. As waters become increasingly nutrient depleted, organisms reduce their discrimination against specific isotopes during uptake and sinking OM increasingly contains higher $\delta^{15}N$ [*Cline and Kaplan*, 1975; *Altabet et al*., 1999]. Once complete nitrate utilization occurs, the $\delta^{15}N$ of OC reflects that of the surrounding water. Carbon isotope signatures are equally complex as light and heavy isotopes are differentially fractionated by C3 and C4 metabolic processes, making it difficult to distinguish terrestrial sources from marine algae if the terrestrial source is comprised of high proportions of C4 plants [*Meyers*, 1994].

Given the multitude of controls on the isotopic composition of sediment, we also assessed the utility of *n*-alkane biomarkers to distinguish sediment source [*Blumer and Clark*, 1967]. Biomarkers are molecular compounds characteristic of a specific organism under a particular set of environmental conditions. Here, we focused on *n*-alkanes as they are generally unreactive, degrade slowly over time, and their chain length typically reflects source. Terrestrial vegetation is characterized by long chain *n*-alkanes (C_{27}, C_{29}, C_{31}, C_{33}), which are utilized for protection and support in leaf waxes [*Meyers*, 2003; *Ficken et al*., 2000]. On the other hand, marine phytoplankton are characterized by short chain *n*-alkanes (C_{15}, C_{17}, C_{19}) and marine macrophytes by mid-length chain *n*-alkanes (C_{21}, C_{23}, C_{25}) [*Meyers*, 2003; *Ficken et al*., 2000]. By measuring the distribution of *n*-alkanes in sediment, the relative contribution from marine and terrestrial sources can be determined.

The objective of this study was to analyze the TOC, TN, the C/N ratio, $\delta^{13}C$ and $\delta^{15}N$ isotopes, and *n*-alkane biomarkers of a well-dated sediment core collected from the center of SBB (previously age dated by *Hendy et al*. [2013]) to elucidate the source of OM to marine sediments during episodic events (e.g., floods and turbidites) and under different climate states (e.g., droughts). Understanding the composition of OC deposited in these sediments by different processes and under various climate conditions provides information regarding how coastal ecosystems may influence global C sequestration.

2. Methods

2.1. Collection and Dating

A sediment core (SPR0901-03KC; 34°16.99'N, 120°2.41'W, Figure 1) was collected from the SBB in January 2009 at a water depth of 586 m [*Hendy et al*., 2013]. Floods, turbidites,

and droughts were identified from Scanning X-Ray Fluorescence (SXRF) elemental analyses [*Hendy et al*., 2015; *Heusser et al*., 2015]. Flood sediments were comprised of high concentrations of lithogenic elements such as titanium (Ti), potassium (K), iron (Fe) and calcium (Ca), and had a high clay content. Drought sediments were comprised of low lithogenic element concentrations. Turbidites were identified by their olive homogenous coloration and larger grain size [*Schimmelmann et al*., 1998; *Hendy et al*., 2013; *Du et al*., 2018]. Following SXRF, the core was sampled at 2 mm intervals and oven dried. An age model was developed using a combination of ^{14}C dating of planktonic foraminiferal carbonates and laminae counts [*Hendy et al*., 2013; *Y. Wang et al.*, 2019]. The age-depth model was generated using Bacon 2.2 [*Blaauw and Christen*, 2011; *Du et al*., 2018], where ^{14}C ages were converted to calendar ages using the Marine13 calibration curve [*Reimer et al*., 2013] with variable reservoir ages from *Hendy et al*. [2013].

Terrestrial end members were defined using river sediment previously collected from dry stream beds during the drought of 2013-2016 [*Napier et al*., 2019] (Figure 1). River sediment from 5 locations were analyzed: the Santa Clara River was sampled at locations 13 (34˚23.10’ N, 118˚47.22’W) and 16 (34˚20.70’N, 119˚01.46’W); the Ventura River was sampled at location 21 (34˚25.20’N, 119˚17.94’W); the Santa Ynez River was sampled at locations 22 (34˚24.60’N, 119˚49.74’W) and 30 (34˚38.40’N, 120˚24.54’W) as described in *Napier et al*. [2019]. The macrophyte end member was defined by a sample of *Macrocystis pyrifera* that was collected from Coal Oil Point in June 2018. Samples were shipped to the University of South Carolina where they were freeze dried and ground prior to analysis.

Sediment traps were utilized to compare sediment core events, such as paleofloods, to modern day flood and background sedimentation. The sediment traps were deployed in the center of the SBB (34°14′N, 120°02′W; Figure 1) at a depth of 500 m in 1993 and continue to the present day [*Thunell*, 1998]. Sediment trap flood samples were selected from the 1997-1998 El Niño flood collected in March-April 1998 [*Bograd et al*., 2001]. Sediment trap samples reflecting background conditions were selected from November 2000 and November 2001 to avoid years associated with flooding, turbidites, or drought.

2.2. Total Organic Carbon, Total Nitrogen, and Isotopic Measurements

For the sediment core, the weight percent TOC (%TOC) and TN (%TN) were measured on Costech ECS 4010 Elemental Analyzer at University of Michigan using the methods of Y. Wang et al. [2019]. For the sediment traps, rivers, and kelp samples, the %TOC and %TN was measured on a Perkin Elmer 2400 CHNS Elemental Analyzer. The standard deviation of TOC and TN measurements for standard replicates was 0.03% and 0.04%, respectively. For OC analyses (TOC and $\delta^{13}C$), inorganic C was removed by acidifying 0.5 mg of sediment with 6 mL of 1 M phosphoric acid, sonicating for 5 minutes, and filtering onto a precombusted GF/F. The filters were dried overnight, folded into 3.0 cm tin disk and pelletized for analysis. For isotopic analysis of C and N, all samples were combusted in a Eurovector Elemental Analyzer connected to an Elementar Isoprime IRMS. Reference materials for ^{13}C were USGS-24, USGS-40, and sucrose. Reference materials for ^{15}N were IAEA-N1 and N2 (ammonium sulfates) and USGS-40. Isotopic measurements are given in reference to a standard; $\delta^{13}C$ was reported relative to Vienna Pee Dee Belemnite (VPDB) with a standard deviation of 0.15‰ and $\delta^{15}N$ was reported relative to atmospheric nitrogen (0‰) with standard deviation of 0.04‰.

2.3. n-Alkane Analyses

Approximately 2 g of homogenized and dried sediment or kelp was used for lipid extraction. Given the large amount of material needed, multiple core intervals of similar isotopic nitrogen signatures were pooled together for extraction, encompassing ~ 1 y for flood and turbidite samples and ~ 8 y for background and drought samples. Lipids were extracted in triplicate by sonicating for 30 min in 50 mL of a 9:1 dichloromethane/methanol (DCM/MeOH) solution and filtering through a GF/F. The extract was concentrated to 2 mL via evaporation under ultrahigh purity nitrogen gas. Sulfur was removed from samples by adding ~ 500 mg activated copper and allowing samples to stand overnight.

The *n*-alkanes were separated from the total lipid extract with silica gel column chromatography. Briefly, the column was packed with 7 cm of silica gel in DCM and 1 cm of anhydrous sodium sulfate to prevent aqueous contamination. The column was made with DCM to minimize contamination that arose from hexane extracting atmospheric contaminants. To switch to a hexane column, the column was loaded with 40 mL of hexane before loading the sample. Once the sample was added, the first fraction (40 mL hexane) was collected for hydrocarbon analysis. This hydrocarbon fraction was evaporated to 500 µL under ultrahigh

purity nitrogen gas and analyzed with a GC/MS. The remaining fractions were stored for future analysis of ketones/esters (40 mL 4:1 hexane/DCM), alcohols (40 mL 9:1 DCM/acetone), and fatty acids (40 mL 12:12:1 DCM/MeOH/formic acid).

Identification and quantification of *n*-Alkanes were conducted using an Agilent 7890B/5977A GC/MS with HP-5MS column outfitted with UHP helium as a carrier gas. One µL of sample was injected into the GC/MS on splitless mode. The initial column temperature was 100°C, increased at a rate of 8°C min^{-1} until 300°C, and remained at 300°C for 23 min. *n*-Alkanes were detected utilizing scanning ion monitoring (SIM) targeting the m/z ion 71, and identified using external standards of known retention times and by analysis of the SIM chromatograms. *n*-Alkane concentrations were determined using external standards (C_{20}, C_{24}, C_{26} and C_{30}) and extrapolating the slopes for the other *n*-alkane chain lengths. Blanks were processed with every batch of seven samples.

A carbon preference index (CPI) was utilized as a proxy for fresh OC [*Bray and Evans*, 1961]. In this study, a modified CPI equation [*Bray and Evans*, 1961; *Scalan and Smith*, 1970; *Pearson and Eglinton*, 2000], was used to encompass the entire spectrum of contributing *n*-alkanes (Equation (1)).

$$CPI = \frac{C_{13}+C_{15}+C_{15}+C_{17}+C_{19}+C_{21}+C_{23}+C_{25}+C_{27}+C_{29}+C_{31}+C_{33}}{C_{14}+C_{16}+C_{18}+C_{20}+C_{22}+C_{24}+C_{26}+C_{28}+C_{30}+C_{32}} \quad (1)$$

The numerator in this equation is the sum of the concentration (µg/g OC) of all odd chain *n*-alkanes from 13 to 33 carbon atoms in length (C_{13}, C_{15}, etc.), and the denominator is the sum of the concentration of all even chain *n*-alkanes from 14 to 32 carbon atoms in length (C_{14}, C_{16}, etc.). Previous work has shown that a higher CPI indicates a greater contribution from fresh organic carbon sources [*Bray and Evans*, 1961]. A lower CPI and increased abundance of even chain *n*-alkanes derive from bacterial degradation and petroleum [*Bray and Evans*, 1961; *Grimalt et al*., 1985].

The burial rates of OC (Equation (2)) and each type of *n*-alkane (Equation (3)) were determined for each type of sedimentation (flood, turbidites, droughts, and background) over the past 2,000 years:

$$OC\ Burial\ Rate(g\ cm^{-1}\ kyr^{-1}) = MAR(g\ cm^{-1}kyr^{-1}) * TOC(\frac{1}{100}) \quad (2)$$

$$n-Alkanes\ Burial\ Rate(\mu g\ cm^{-1}\ kyr^{-1}) = OC\ Burial\ Rate * n-alkane(\frac{\mu g}{gTOC}) \quad (3)$$

The above equations utilized sediment mass accumulation rate (MAR; g cm^{2-} y^{-1}; Equation (4)), %TOC (1/100), and *n*-alkane concentration (µg/g OC). The *n*-alkane burial was separated into three categories based on chain length (algal, macrophyte, or terrestrial). Organic C and *n*-alkane burial during each type of sedimentation were compared to the total OC and *n*-alkanes buried over the past 2,000 years (Equation (5)).

$$MAR(g\ cm^{-1}\ kyr^{-1}) = \text{Linear sedimentation rate (cm kyr}^{-1}) * \text{Dry Bulk Density (g cm}^{-3}) \quad (4)$$

$$\%OC\ Buried = \frac{OC\ Burial\ of\ Sedimentation\ Type\ (i.e. flood, drought, turbidite, or\ background.)}{Sum\ of\ OC\ Burial\ for\ Every\ Sedimentation\ Type}\ x\ 100 \quad (5)$$

2.4. Statistical Analysis

Significant differences between samples were determined using a one tailed Student's t-test assuming unequal variances where $\alpha < 0.05$. These statistical analyses allowed for gross characterization of events (i.e., flood versus background). While this study may suggest transport mechanisms to the ocean floor, we did not account for any transformations that may have occurred in the water column. We also assume that there was no preferential degradation of specific *n*-alkanes within the water column or sediment (See Section 4.4).

3. Results

Flood events are identified in the sediment core by SXRF as having high concentrations of lithogenic-associated elements, Ti and Fe, and low concentrations of the biogenic-associated element, Ca [*Hendy et al*., 2015; *Du et al*., 2018]. Drought intervals are identified by low concentrations of lithogenic elements and high concentrations of biogenic Ca and Si [*Hendy et al*., 2015]. Turbidite sediment is visually characterized by a homogenous olive coloration and larger grain size, and are derived from turbidity currents stimulated by mass failure on the basin slope [*Rack and Merill*, 1995; *Schimmelmann et al*., 1998; *Hendy et al*., 2015; *Du et al*., 2018].

319

320 *3.1. TOC, TN, C/N, and Isotopic Results*

321 Flood sediment has significantly lower average TOC, TN, $\delta^{13}C$ and $\delta^{15}N$ relative to
322 background sediment ($p < 0.001$), and a significantly higher molar C/N ratio ($p < 0.001$; Table 1,
323 Figure 2). These results are in excellent agreement with SXRF derived trace element
324 measurements used to identify floods [*Hendy et al*., 2015] (Figure 3). Turbidites contain a
325 mixture of flood and background sediment characteristics, with TOC and TN concentrations
326 significantly different from flood and background sedimentation ($p < 0.001$). Turbidites have
327 C/N ratios and $\delta^{15}N$ signatures similar to background sediment, while the turbidite $\delta^{13}C$ signature
328 is significantly lower ($p < 0.001$). Drought intervals are nearly indistinguishable from
329 background sediment with regards to TOC, TN, and C/N ratios.

330 **Table 1:** Average relative abundance of Total Organic Carbon (TOC), and Total Nitrogen (TN) and
331 molar C/N ratios and isotopic composition in Santa Barbara Basin sediments and sediment end members.

	Background	**Drought**	**Flood**	**Turbidite**	**Kelp**	**Sediment Trap Background**	**Sediment Trap Flood**
	n=33	*n=25*	*n=58*	*n=34*	*n=1*	*n=2*	*n=2*
TOC (wt %)	3.70 ± 0.31	3.90 ± 0.25	2.13 ± 0.53	2.98 ± 0.23	13.79	3.79 ± 0.25	3.53 ± 1.87
TN (wt %)	0.41 ± 0.04	0.44 ± 0.03	0.22 ± 0.06	0.33 ± 0.03	1.04	0.48 ± 0.07	0.52 ± 0.31
C/N	10.67 ± 0.47	10.34 ± 0.28	11.45 ± 1.03	10.63 ± 0.55	15.47	9.27 ± 0.75	8.12 ± 0.67
$\delta^{13}C$ (‰)	-21.9 ± 0.09	-21.98 ± 0.09	-24.34 ± 0.84	-22.5 ± 0.21	-14.73	-21.01 ± 0.64	-22.12 ± 0.16
$\delta^{15}N$ (‰)	7.54 ± 0.20	7.88 ± 0.09	6.26 ± 0.84	7.59 ± 0.21	9.79	7.87 ± 0.19	6.62 ± 0.21

332

333

334

335

336

337

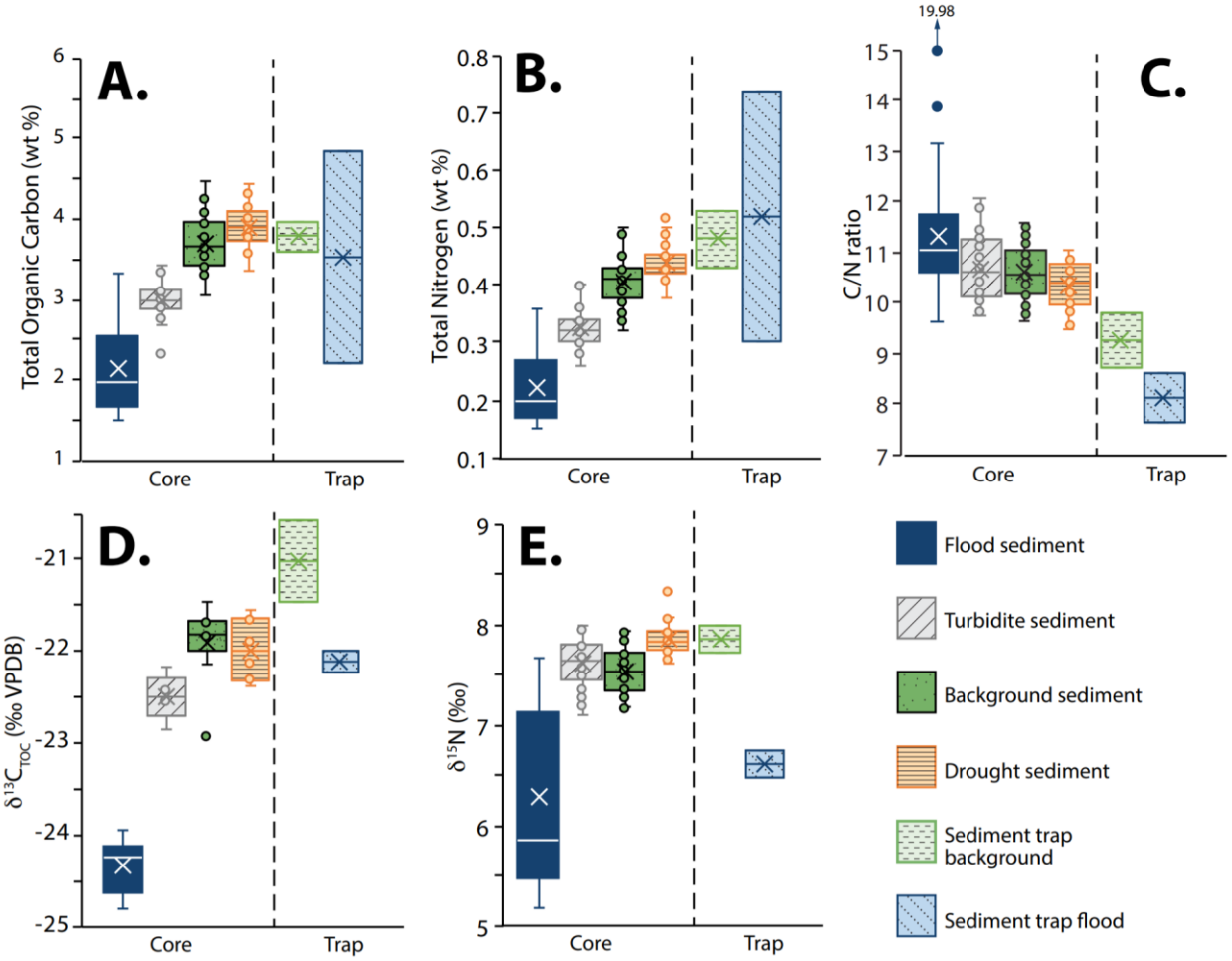

Figure 2: Box plot comparisons of composition by sediment type: Flood (dark blue solid box), turbidites (pale gray diagonal striped box), background (dark green speckled box), and drought (orange horizontal striped box) sediments relative to sediment trap background (pale green dashed box) and flood (pale blue dashed horizontal striped box) for **A.** Total Organic Carbon (weight %), **B.** Total Nitrogen (weight %), **C.** C/N ratio, **D.** $\delta^{13}C$ (‰ SMOW) and **E.** $\delta^{15}N$ (‰). Within each box, the line is the median, the X is the mean, and points outside of the boxes (greater than 1.5 quartiles) are outliers.

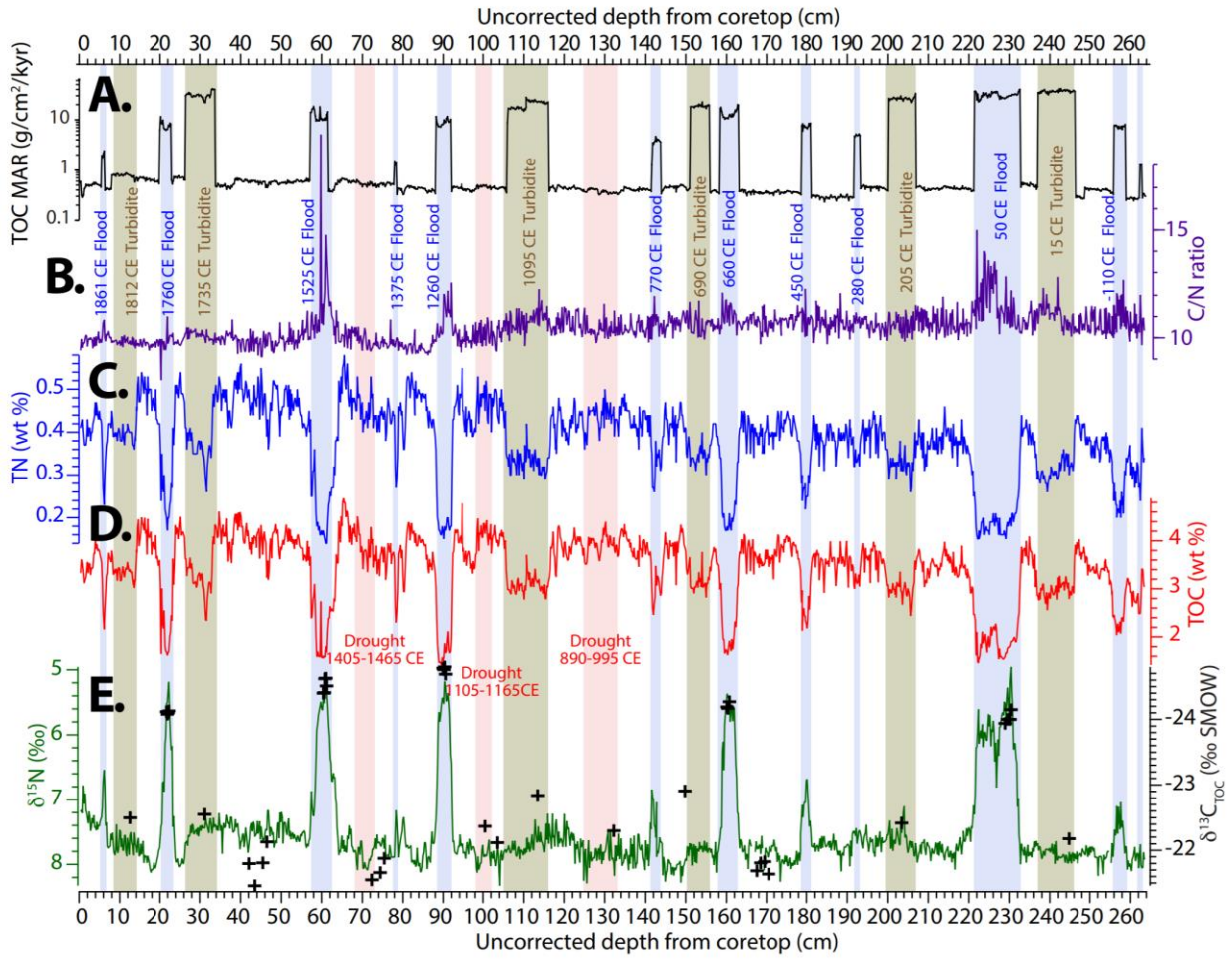

Figure 3: Uncorrected depth profiles spanning the past 2,000 years from the SBB sediment record. **A.** Total Organic Carbon (TOC) Mass Accumulation Rates (MAR) (g, cm^{-2}, kyr^{-1}; black line), **B.** Molar C/N ratio (purple line), **C.** Total Nitrogen (TN) (weight %; blue line), **D.** Total Organic Carbon (TOC) (weight %; red line), and **E.** $\delta^{13}C$ (‰ SMOW; black crosses) and $\delta^{15}N$ (‰; green line) vary during instantaneous events, such as flooding (blue shaded bars), turbidites (tan shaded bars) [*Du et al*., 2018], and droughts (red shaded bars) [*Heusser et al*., 2015].

Sediment trap samples collected during and after the 1997-1998 El Niño are analyzed to constrain recent flood and background source signatures in the SBB. Sediment trap TOC and TN concentrations are highly variable, particularly during flood periods, and both flood and background sediment trap material are significantly higher than those measured in flood sediments. Flood sediment trap C/N is significantly lower than flood sediment ($p < 0.01$) and background sediment trap C/N is lower than that measured in core background sediment ($p =$

0.06). The $\delta^{13}C$ signatures of both background and flood sediment trap material are similar to background sediments. In contrast, the $\delta^{15}N$ signature of the flood sediment trap is indistinguishable from that measured in flood sediments, again supporting the use of $\delta^{15}N$ as a tracer of flood events.

Kelp is measured to constrain the inputs of macrophytes to the basin while sediment from each of the rivers are measured to constrain the terrestrial end member. Kelp is characterized by a higher C/N ratio, $\delta^{13}C$, and $\delta^{15}N$ (Table 1). While the C/N ratios for each river are similar, the isotopic composition is more variable; $\delta^{13}C$ ranges from -31.53‰ to -22.80‰ and $\delta^{15}N$ ranges from 4.41‰ to 8.51‰ (Table 2). Nonetheless, average $\delta^{13}C$ and $\delta^{15}N$ signatures of river sediments are consistent with those measured in flood sediments.

Table 2: Relative concentrations of Total Organic Carbon (TOC), Total Nitrogen (TN), *n*-alkanes, C/N ratios and isotopic composition of bed load sediments in rivers draining into the Santa Barbara Basin.

Location Number*	**13** **Santa Clara River**	**16** **Santa Clara River**	**21** **Ventura River**	**22** **Santa Ynez River**	**30** **Santa Ynez River**	**Average River Sediment**
Latitude, Longitude	34°23.10'N, 118°47.22'W	34°20.70'N, 119°01.46'W	34°25.20'N, 119°17.94'W	34°24.60'N, 119°49.74'W	34°38.40'N, 120°24.54'W	--
C_{25} (µg/gOC)	6	BDL	BDL	7	12	5 ± 5
Terrestrial C_{27}, C_{29}, C_{31} (µg/gOC)	147	146	820	118	192	285 ± 269
TOC	2.68	0.43	0.87	2.13	1.15	1.45 ± 0.93
TN	0.25	0.07	0.12	0.19	0.14	0.15 ± 0.07
C/N	12.51	7.17	8.46	13.08	9.58	10.16 ± 2.56
$\delta^{13}C$ (‰)	-24.77	-31.53	-22.80	-27.10	-24.05	-26.05 ± 3.44
$\delta^{15}N$ (‰)	7.00	8.51	4.41	6.28	6.30	6.50 ± 1.48

* Sample location description in *Napier et al*. [2019]

3.2. n-Alkanes

The *n*-alkane composition of kelp is used to characterize the macrophyte end member, while the terrestrial end member is constrained using river samples collected during a drought period. During a drought, riverine sediment is likely dominated by terrestrial vegetation adapted to low water conditions as riverine algae is minimal due to dry stream beds. As such, this end member may not be fully representative of the terrestrial end member during floods. River

sediment contain 94-100% long chain *n*-alkanes and range in concentration from 118 to 820 µg/g OC (Table 2). These river sediments are in agreement with previously reported terrestrial *n*-alkane compositions [*Meyers*, 2003; *Ficken et al.*, 2000]. Kelp contains mid-chain *n*-alkanes, C_{21} and C_{23}, but did not contain C_{25}. However, the Santa Clara and Santa Ynez Rivers did contain the *n*-alkane, C_{25}, most likely due to river macrophytes that the Ventura River lacked (Table 2). We therefore exclude C_{25} from our marine macrophyte end member analyses to remove the potential freshwater influence.

Table 3: Concentration of *n*-alkanes in Santa Barbara Basin sediments and end members.

	Background *n=7*	**Flood** *n=12*	**Turbidite** *n=6*	**Drought** *n=5*	**Kelp** *n=1*	**Sediment Trap Background** *n=2*	**Sediment Trap Flood** *n=2*	**Rivers** *n=5*
CPI	2.41 ±1.90	3.47 ± 1.67	4.08 ± 4.79	2.78 ± 2.45	2.12	5.96 ± 2.34	3.33 ± 1.12	Only Odds
Algal C_{15}, C_{17}, C_{19} (µg/gOC)	6 ± 5	11 ± 13	7 ± 3	7 ± 7	16	20 ± 22	27 ± 11	BDL
Macrophyte C_{21}, C_{23} (µg/gOC)	2 ± 3	5 ± 7	3 ± 3	4 ± 6	7	5 ± 7	BDL	BDL
Terrestrial C_{27}, C_{29}, C_{31} (µg/gOC)	23 ± 13	70 ± 42	23 ± 14	15 ± 7	BDL	30 ± 7	40 ± 33	285 ± 300

Flood events are characterized by higher total *n*-alkane concentrations and greater changes in the relative *n*-alkane composition. Terrestrial *n*-alkane (C_{27}, C_{29}, C_{31}, C_{33}) concentrations in flood sediments are significantly higher than those measured in background sediments (81% versus 75% of total *n*-alkanes, $p = 0.001$) (Table 3; Figures 4, 5 and 6). Flood events are also characterized by approximately double the concentration of macrophyte *n*-alkanes (C_{21}, C_{23}) and algal *n*-alkanes (C_{15}, C_{17}, C_{19}) compared to background sediment, although concentrations were highly variable within each classification ($p = 0.11$, $p = 0.10$) (Figures 4, and 5). Higher concentrations of representative biomarker *n*-alkanes (i.e., terrestrial, macrophyte, and the algal *n*-alkanes) strongly correlate with the lower $\delta^{15}N$ isotopic signatures measured in flood sediments (Figure 4). Flood events are also characterized by higher CPI ratios relative to background sediment, but this difference is not significant due to the high variability in the measurements ($p = 0.13$).

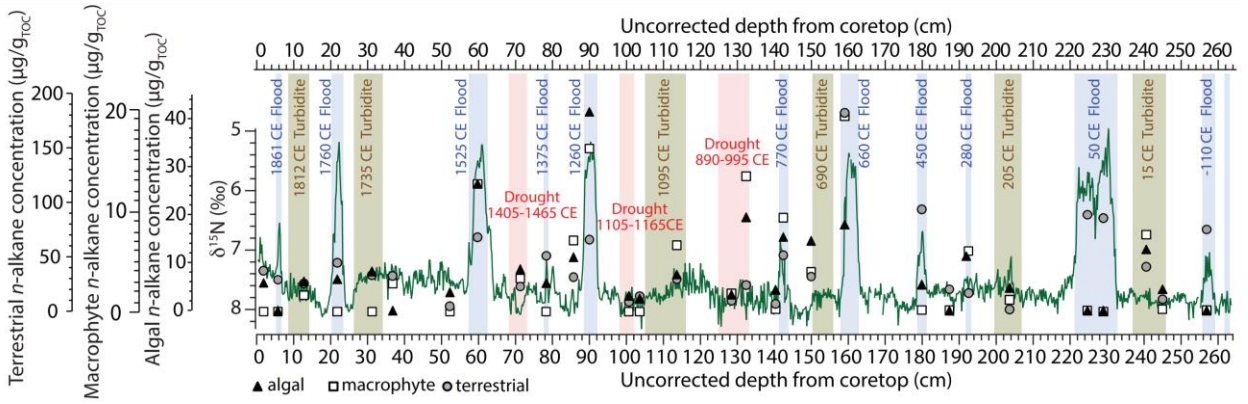

Figure 4: Comparison of 2,000 years of $\delta^{15}N$ (‰; green line) and *n*-alkane concentrations normalized to TOC (µg/g TOC) by depth in sediment core. The concentration of terrestrial (C_{27}, C_{29}, C_{31}, C_{33}; grey circles), macrophyte (C_{21}, C_{23}; white squares) and algal (C_{15}, C_{17}, C_{19}; black triangles) *n*-alkanes varies during instantaneous events such as flooding (blue bars), and turbidites (tan bars) [*Du et al*., 2018] as well as during droughts intervals (pink bars) [*Heusser et al*., 2015]. Note: *n*-alkane concentrations depicted as 0 are Below Detection Limit (BDL) of 0.5 mg/L in hexane on the GC/MS.

Turbidite terrestrial and algal *n*-alkane composition are most similar to background sediment (Table 3; Figure 5). Turbidites also have a macrophyte concentration indistinguishable from either background or flood sediment ($p = 0.17$). Drought sediments are characterized by the lowest CPI and terrestrial *n*-alkane concentration of all of the sediments measured (Table 3, Figure 5). Terrestrial *n*-alkanes comprise just 58% of the total *n*-alkane composition in droughts, while algal *n*-alkanes are the highest of all of the sediment types measured, 28% of the total *n*-alkane signal (Figure 6).

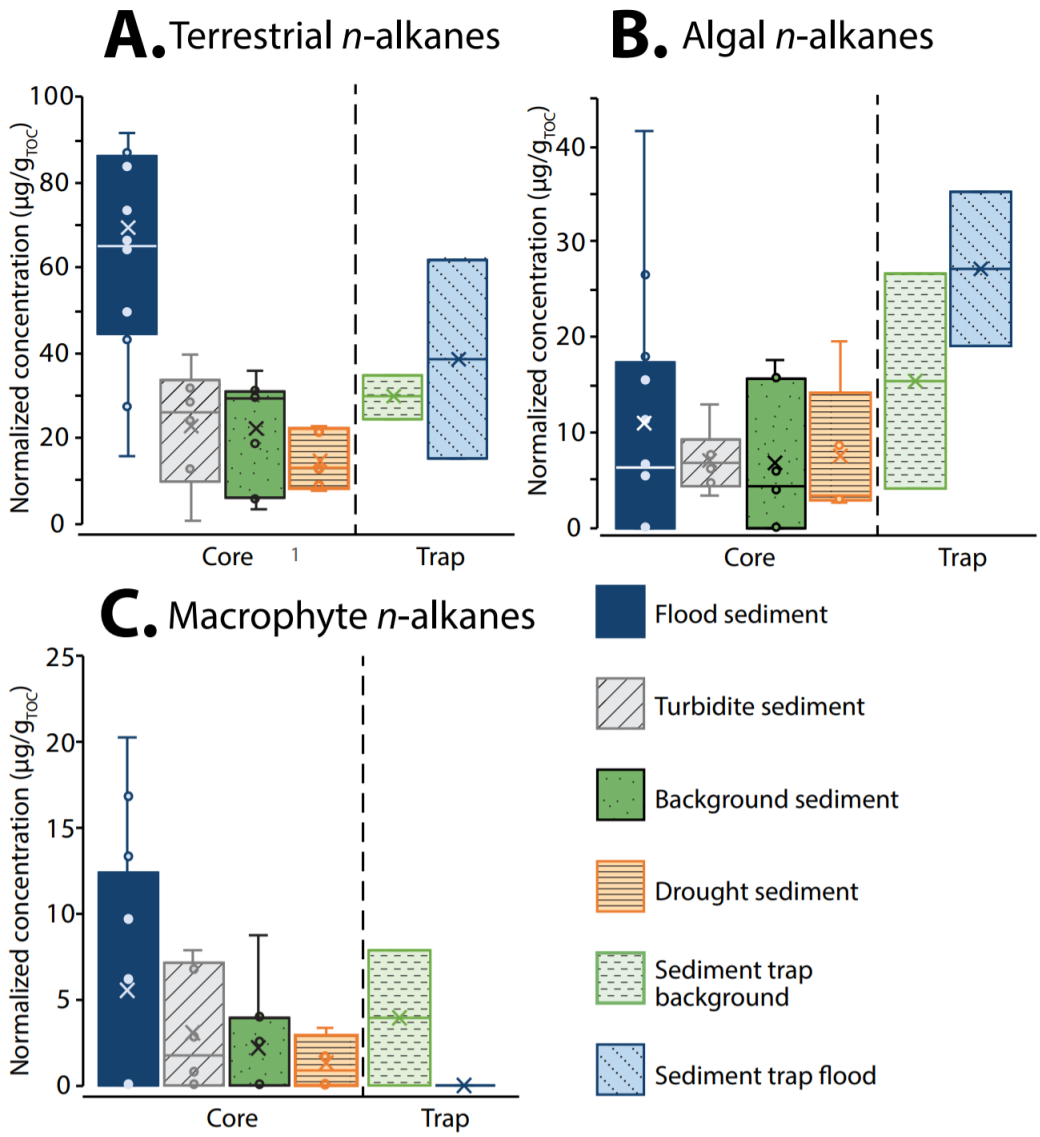

Figure 5: Box plot comparison of normalized concentrations (µg/g TOC) of *n*-alkane source by sediment type: Flood (dark blue solid box), turbidites (pale gray diagonal striped box), background (dark green speckled box), and drought (orange horizontal striped box) sediments relative to sediment trap background (pale green dashed box) and flood (pale blue dashed horizontal striped box) material for **A.** terrestrial (C_{27}, C_{29}, C_{31}, C_{33}), **B.** algal (C_{15}, C_{17}, C_{19}), and **C.** macrophyte (C_{21}, C_{23}) *n*-alkanes. Within each box, the line is the median, the X is the mean, and points outside of the box are outliers.

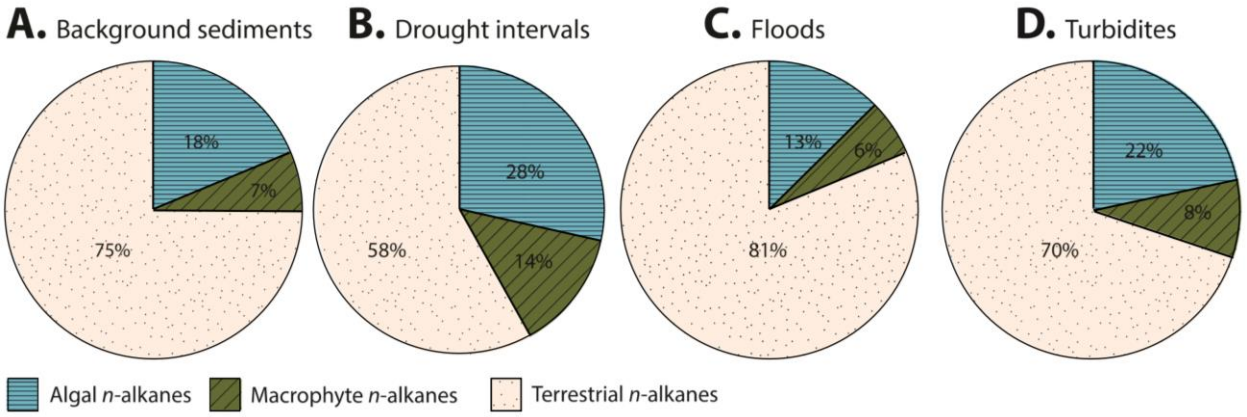

Figure 6: The relative contribution of *n*-alkane sources in Santa Barbara Basin sediments: **A.** background sediments, **B.** drought intervals, **C.** flood events, and **D.** turbidites. Terrestrial *n*-alkanes (C_{27}, C_{29}, C_{31}, C_{33}; tan, speckled shading) dominate all sediment types. Macrophyte *n*-alkanes (C_{21}, C_{23}) are depicted by the dark green shading with diagonal lines, and algal *n*-alkanes (C_{15}, C_{17}, C_{19}) are depicted by the blue shading with horizontal lines.

Sediment trap samples are dominated by terrestrial *n*-alkanes followed by a large contribution of algal *n*-alkanes (Table 3, Figures 5 and 6). Macrophyte *n*-alkane concentrations, however, are low for both flood and background sediment traps; flood sediment macrophytes are below detection. Overall, sediment traps have higher abundances of algal *n*-alkanes compared to the sediment core background ($p = 0.05$). The sediment trap flood CPI is indistinguishable from the flood sediment, however the sediment trap background CPI is more than double that of the sediment background. We attribute this difference to the reduced elapsed time available for degradation in the sediment trap (weeks versus years).

3.3 Total Organic Carbon Burial

The average sedimentation rate for SBB background sediment is 0.95 ± 0.19 mm y^{-1} and the TOC burial rate is 0.43 ± 0.09 g cm^{-2} ky^{-1} (Table 4). The sedimentation rate significantly increases in both flood ($p = 0.01$) and turbidite layers ($p = 0.01$), which are assumed to be geologically instantaneous. The sediment accumulation rate for flood sediment is 38.30 ± 34 mm y^{-1} and has a TOC burial rate of 11.52 ± 8.90 g cm^{-2} ky^{-1}. The sedimentation rate for turbidities is 61.74 ± 32.00 mm y^{-1}, with an OC burial rate of 24.37 ± 12.40 g cm^{-2} ky^{-1}. Conversely, the sedimentation rate and mass accumulation rate for drought sediment are nearly half that of background sediment ($p = 0.01$).

Table 4: Sedimentation and burial rates in Santa Barbara Basin sediments.

		Sedimentation Rate (mm, yr^{-1})	Mass Accumulation Rate (g, cm^{-2}, yr^{-1})	OC Burial Rate (g, cm^{-2}, kyr^{-1})	Terrestrial Burial Rate (µg, cm^{-2}, kyr^{-1})	Macrophyte Burial Rate (µg, cm^{-2}, kyr^{-1})	Algal Burial Rate (µg, cm^{-2}, kyr^{-1})
Background	*n = 7*	0.95 ± 0.19	0.0236 ± 0.04	0.43 ± 0.09	9.61 ± 6.27	0.84 ± 1.22	2.43 ± 0.10
Drought	*n = 5*	0.85 ± 0.14	0.0107 ± 0.002	0.42 ± 0.07	6.41 ± 3.27	1.35 ± 1.93	2.99 ± 2.54
Flood	*n = 12*	38.30 ± 34*	0.6205 ± 0.51	11.52 ± 8.9	439 ± 612	37.3 ± 74.4	67.6 ± 112
Turbidite	*n = 6*	61.74 ± 32*	0.8359 ± 0.45	24.37 ± 12.4	578 ± 548	72.2 ± 111.8	188 ± 155

* Assuming each event has a duration of one year.

Due to the prolonged and relatively low sedimentation rates, background and drought sediments are combined into a "non-event" sedimentation category. Non-event sedimentation is responsible for 75% of the TOC buried over the past 2,000 years (Figure 7). Of the different classes of *n*-alkanes measured, non-event sedimentation is responsible for 72% of total algal OC buried, 58% of macrophyte OC buried, and 59% of terrestrial OC buried. Flood events account for 11 of the past 2,000 years (less than 1% of time and assuming instantaneous burial) and are responsible for 8% of the TOC buried. Floods contribute 14% of the total algal OC buried, 28% of the total macrophyte OC buried, and 31% of the total terrestrial OC buried over the past 2,000 years. Turbidites account for 6 of the 2,000 years studied (less than 1% of time) and are responsible for remobilizing 13% of the total OC buried over the past 2,000 years and buried 14% of the total algal OC, 15% of the total macrophyte OC, and 10% of the total terrestrial OC in the deep basin. It is important to note that the above estimates assume that *n*-alkanes are representative of the bulk OC deposited and buried from a specific source (See Section 4.4).

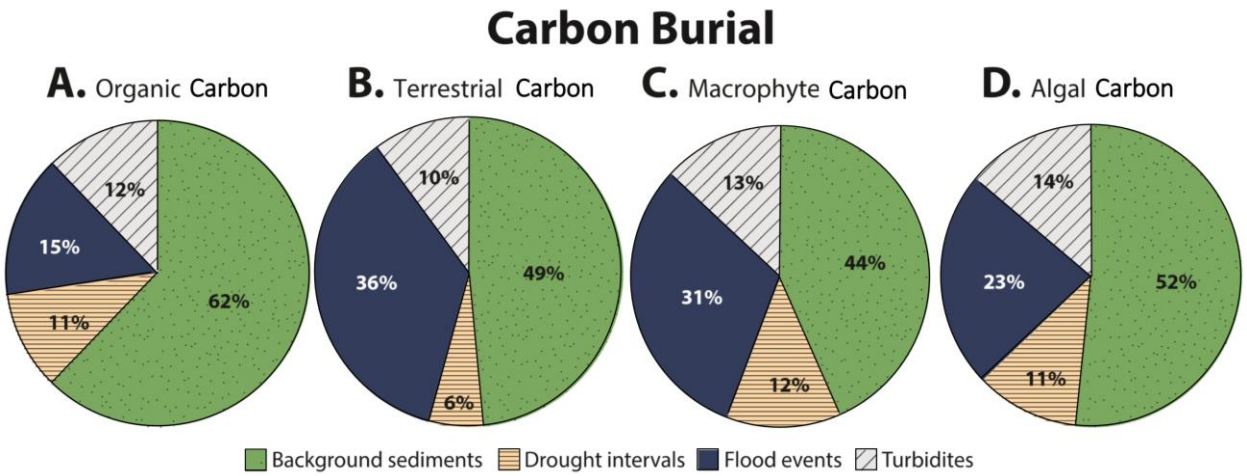

Figure 7: The relative contribution of each sediment type to burial of Total Organic Carbon and different *n*-alkane sources in SBB sediments. Carbon burial is divided into: **A.** organic carbon, **B.** terrestrial (C_{27}, C_{29}, C_{31}, C_{33}) carbon, **C.** macrophyte (C_{21}, C_{23}) carbon, and **D.** algal (C_{15}, C_{17}, C_{19}) carbon, where green speckled shading represents background sediments, tan horizontally striped shading represents drought intervals, dark blue shading represents flood events sediments and grey diagonal shading represents turbidites.

4. Discussion

4.1 Terrestrial Sourced Organic Matter Dominates Flood Sediment

All flood sediments were dominated by terrestrially sourced OM. Sediments from flood periods contained significantly lower TOC and had the most depleted $\delta^{13}C$ (-24.34 ± 0.84 ‰) and $\delta^{15}N$ (6.26 ± 0.84‰) values (Figures 2 and 3), consistent with non-marine sources of organic matter [*Sweeney and Kaplan*, 1980; *Meyers*, 1994]. The $\delta^{15}N$ signature of flood sediments is significantly lower than background, turbidite, and drought sediments, with fluctuations of > 1.5‰ that are substantially greater than the ± 0.5‰ (Figure 3E) associated with changes in water column mixing, biological utilization, and oxygen availability (e.g., *Y. Wang et al.*, 2019, See Section 1.2). These flood sediments, however, are not as depleted as the ~ 2‰ reported by *Sweeney and Kaplan* [1980] in terrestrial sewage effluent, suggesting a mixed marine and sediment source. In addition, *n*-alkane concentrations from terrestrial sources (e.g., long chain length *n*-alkanes C_{27}, C_{29}, and C_{31}) are almost three times higher than that measured in background sediments and are 81% of the total *n*-alkanes measured (Table 3, Figures 5 and 6). These results are consistent with previous work showing that long chain *n*-alkanes dominate the

n-alkane composition of SBB sinking particles and sediments [*Bray and Evans*, 1961; *Crisp et al*., 1979]. Finally, terrestrial OM sources in flood sediments are also in agreement with lithogenic element concentrations that indicate terrestrial origins [*Hendy et al.*, 2015]. Combined, these results support our conclusions that a substantial component of flood sediments is derived from terrestrial OM.

The most likely source of the terrestrially derived OM in flood sediments is the numerous rivers that drain into the SBB. The Santa Clara River is considered to be the dominant contributor of basin sediment since it has the highest riverine discharge and generally carries the largest sediment load [*Warrick et al.*, 2005]. The Santa Clara and Santa Ynez Rivers have low $\delta^{13}C$ values characteristic of terrestrial OC ($\delta^{13}C < -31.5‰$, Table 2). However, the $\delta^{15}N$ of flood event sediments is most similar to the $\delta^{15}N$ of the Santa Ynez and Ventura River sediments ($\delta^{15}N < 6.3$ ‰). These $\delta^{15}N$ isotopic values are consistent with inorganic analyses of river sediments that indicate that the 1861-62 and 1761 AD flood events contain lithogenic sediment derived from the southern slopes of the Santa Ynez and Topatopa Mountains that lie in the Santa Ynez and Ventura River catchments [*Napier et al*., 2019]. Therefore, based on the combined $\delta^{13}C$ and $\delta^{15}N$ results, the Santa Ynez and Ventura Rivers potentially contribute more terrestrial sediment to SBB during floods than during intervals of background sedimentation.

Terrestrial material is likely transported into the SBB via two different pathways. During winter rainfall and flood events, sediment is dispersed in both surface waters and subsurface hyperpycnal plumes that are transported to the center of the SBB [*Thornton*, 1984, 1986; *Thunell*, 1998; *Warrick et al*., 2007; *Warrick and Farnsworth*, 2009]. These subsurface hyperpycnal flows of denser material may bypass the sediment traps deployed shallower in the water column and may explain differences between flood sediments and sediment trap material [*Mulder and Syvitski*, 1995]. Another mechanism is associated with spring blooms (*Thunell*, 1988). Terrestrial (also termed lithogenic) particles typically have smaller grain sizes that sink more slowly. During the spring, these small particles scavenge onto larger biogenic particles and thus sink rapidly to the seafloor [*Thunell*, 1998; *Ransom et al.*, 1998]. This hypothesis is supported by data presented by *Davis et al*. [2019], who measured a lower $\delta^{15}N$ signal associated with terrestrially derived OM in deep sediment trap material (500 m) during the spring bloom.

During deposition of flood layers, extremely high precipitation rates lead to increased river discharge and deliver more terrestrial material to the continental margin over short time

intervals, increasing sedimentation rates (Figure 7, Table 4) [*Ropelewski and Halpert*, 1989; *Warrick and Farnsworth*, 2009]. These higher sedimentation rates are also characterized by lower TOC and TN concentrations due to dilution of less OM rich terrestrial material (Table 1). The average sedimentation rate across the entire SBB record is ~1 mm y^{-1} (mass accumulation rate = 0.0236 ± 0.04 g cm^{-2} y^{-1}) [*Emery and Hülsemann*, 1962; *Thunell*, 1998; *Emmer and Thunell*, 2000] with the sedimentation rate decreasing during drought intervals [*Du et al.*, 2018]. Assuming each flood layer is deposited as a single event spanning a year, the average sedimentation (and mass accumulation) rates increase during floods by a factor of thirty (e.g., Table 4, Figure 7) [Emery and Hülsemann, 1962; Thunell, 1998; Emmer and Thunell, 2000]. Some flood layers (e.g., 53 A.D.) are considerably thicker than others (Figure 3) resulting in sediment and mass accumulation rates two orders of magnitude higher than most flood events. These rates should be considered maxima, as flood events may occur over several years or more, potentially resulting in lower accumulation rates. Despite the lower TOC concentrations, flood events are still responsible for burying OC at a rate > 25 times faster than that of background and drought periods. Therefore, flood events have the capacity to rapidly bury large amounts of terrestrial OC, and likely play an important role in carbon sequestration on continental margins.

4.2 *Turbidites*

Turbidites appear to be a mixture of terrestrial and marine biogenic material. In addition to having significantly lower average $\delta^{13}C$ signatures (-22.57 ± 0.25‰) relative to background and drought sediments ($p < 0.001$), they also have lower TOC and TN concentrations, consistent with dilution by terrestrial material as evidenced by Hendy et al. [2015]. The $\delta^{15}N$ signatures and terrestrial *n*-alkane concentrations of turbidites, however, are not significantly different from those measured in background sediments (Tables 1 and 3; Figures 2 and 5). We hypothesize that turbidites remobilize oxygenated shelf sediments with a larger concentration of terrestrial material and transport it into the deep basin. Once in the deep basin, Schimmelmann et al. [2013] found that surface sediment may be resuspended prior to the turbidity current settling on the seafloor. While the resuspension and mixing of material may contribute to the similarity in $\delta^{15}N$ between turbidtes and background sediment, we hypothesize that this is unlikely since the age model surrounding the turbidite deposits was not disrupted [*Hendy et al*., 2013].

Turbidites result in an instantaneous sedimentation rate of 61.74 ± 32 mm y^{-1} (Table 4). This is comparable to previously measured turbidite sedimentation rates in the SBB [*Soutar et al*., 1977]. Turbidite mass accumulation rates are the highest of all the sediment types measured, reaching 0.84 g cm^{-2} y^{-1}, 30% higher than that measured in flood sediments, and 40 times higher than that measured in background and drought sediments (Figure 7). The rates of TOC burial in turbidites are double that measured in flood events, and more than 50 times higher than measured in background and drought sediments due to the higher TOC concentrations measured in turbidite sediments.

4.3 All Sediments Contain Marine Sourced Organic Matter

Although terrestrial material is important in both flood and turbidite samples, all of the sediment types analyzed in this study contain marine derived OM. The magnitude of this marine contribution, however, varies across sediment types and is most evident in the $\delta^{13}C$ and $\delta^{15}N$ sediment signatures, and the relative marine algal and macrophyte *n*-alkane abundances. Background and drought sediments have $\delta^{13}C$ signatures of ~ 22‰, consistent with marine phytoplankton versus vascular land plants [*Sweeney and Kaplan*, 1980; *Meyers*, 1994]. The $\delta^{15}N$ signatures of background, turbidite and drought sediments are also consistent with the ~ 7.5‰ measured in open ocean marine OM [*Sweeney and Kaplan*, 1980] and the ~ 7.88‰ measured by *Emmer and Thunell* [2000] in SBB sediments over the past 15,000 years.

Variability within $\delta^{15}N$ sediment signatures may point to larger scale changes in SBB hydrography. Smaller variations in $\delta^{15}N$ signatures of < 1.5 ‰ between turbidite layers (Figure 3) are likely due to differences in the relative magnitude of terrestrial OM remobilization during each event. In contrast, variations in background and drought $\delta^{15}N$ signatures are likely due to larger scale oscillations in water column mixing, biological utilization, and oxygen availability [*Emmer and Thunell*, 2000; *Hendy et al*., 2004; *Tems et al*., 2015; *Y. Wang et al*., 2019] as terrestrial inputs during drought periods should be minimized with decreased freshwater flow (as also supported by *n*-alkane composition, see Figure 6). Previous work shows a strong coherence between $\delta^{15}N$, TOC, and drought in the SBB during the past 2000 years [*Y. Wang et al.*, 2019]. They attribute this strong relationship to an increase in SBB upwelling intensity that is hypothesized to occur in response to the position and strength of the North Pacific High atmospheric pressure system. This change in atmospheric circulation suppresses rainfall and

creates persistent northerly winds that drive upwelling and OM export on the California Margin (Checkley & Barth, 2009). Enhanced equatorial upwelling associated with stronger trade winds may also lead to expansion of the oxygen minimum zone (OMZ) in the Eastern Tropical North Pacific due to increased OM remineralization [*Deutsch et al*., 2014]. As the OMZ expands, the $\delta^{15}N$ of nitrate also increases and this signal could potentially be advected from the Eastern Tropical North Pacific into the SBB by the California Undercurrent.

The *n*-alkane composition of each sedimentation type provides an additional indicator of both marine and macrophyte algae inputs to deep basin sediments. Short chain *n*-alkanes are typically derived from non-vascular plant sources, and here, represent marine derived algal material. Macrophyte *n*-alkanes, or mid-chain length *n*-alkanes, are most likely derived from giant kelp, *Macrocystis pyrifera*, which is abundant along the SBB shoreline [*Schimmelmann and Tegner*, 1991]. Background sediments had the lowest concentrations of algal and macrophyte *n*-alkanes compared with flood and turbidite sediments. Drought sediments have similar marine algal and macrophyte *n*-alkane concentrations, but higher relative percentages of these constituents due to the lower abundance of terrestrial *n*-alkanes, consistent with reduced river runoff derived sediment during low rainfall years (Figure 6). Combined, marine sources of *n*-alkanes account for < 42% of the total *n*-alkanes measured, and the variability in the relative percentage of this marine component is mainly due to the fluctuating amount of terrestrial derived *n*-alkanes in the different types of sediments.

While flood sediments are dominated by terrestrial signatures (see Section 4.1), algal and macrophyte *n*-alkane concentrations, although variable, remain the highest in flood sediments, with a ~ 2 to 3-fold increase relative to the other sediments (Table 3). During floods, the higher algal signal is likely the result of increased riverine discharge carrying more nutrients into the SBB or storm-related mixing bringing more nutrients from depth into the photic zone, as both stimulate phytoplankton growth [*Wrobleski and Richman*, 1987; *Ogston and Sternberg*, 1999; *Otero and Siegel*, 2004; *Warrick et al*., 2005, *Waliser and Guan*, 2017]. Previous work by *Warrick et al*. [2005] in the SBB, found that episodic rain events increase nutrient discharge into the basin. Furthermore, they found that algal biomass was highest in the surface waters of the central basin rather than in the mouth of the Santa Clara River, which would suggest that the algal signal is predominantly derived from marine algae rather than freshwater. A marine algal

signal is further confirmed by the river end members, which did not show any algal material present, although they were not collected during a flood event.

Flood, and to a lesser extent, turbidite sediments contain marine macrophyte *n*-alkanes (mid-chain length, C_{21}, C_{23}) concentrations that are higher than those measured in drought and background sediments ($p = 0.10$; $p = 0.17$). In flood sediments, marine macrophyte contributions are variable, ranging from about double those measured in the other sediment types (Table 3, Figure 5) to below detection. Kelp can die due to age, grazing, or destruction by waves prior to being deposited on the ocean floor [*Cavanaugh et al.*, 2011]. Severe storms and floods have been observed to cause widespread destruction of kelp forests, substantially reducing their biomass [*Schimmelmann and Tegner*, 1991]. Based on our data, we hypothesize that flood-producing storms can be associated with kelp forest destruction with their remains transported into the deep basin where the OC is incorporated into the sediments. Since not all flood events contained macrophyte *n*-alkanes, we hypothesize that some storm induced transport is weaker, minimizing kelp die-off. This hypothesis is supported by low macrophyte concentrations, which also correlate strongly with low algal concentrations in flood sediments ($R^2 = 0.77$, data not shown), suggesting weaker ocean mixing or river discharge during those events. Therefore, even though the kelp itself does not originate from land, the processes that transport large quantities of material off shore (e.g., floods and turbidites) also carry significant quantities of kelp-derived material.

4.4. Utility of n-Alkanes Proxy for Sediment Source

Lipid biomarkers, specifically *n*-alkanes, were chosen as a potential proxy for sediment source due to their known resistance to degradation compared to other forms of OM containing nitrogen and phosphorus [*Eglinton et al.*, 1991*; Meyers and Ishiwatari*, 1993]. Of the lipid biomarkers typically used (e.g., *n*-alkanes, ketones, alcohols, and fatty acids), the *n*-alkane class is the least reactive and slowest to degrade [*Wakeham et al*., 1997]. Constraining *n*-alkane degradation by chain length has been challenging due to the variety of factors that influence degradation in the water column and sediments, including redox, salinity, temperature, pressure, sediment matrix, and microbial community composition [*Schwarz et al., 1974; Canuel and Martens 1996*; *Lamontagne et al., 2004*; *Lofthus et al., 2018*; *B. Wang et al., 2019*]. For example, during transport and arrival at the seafloor, *n*-alkanes have been shown to be a potential energy

source under both aerobic and anaerobic conditions [*Caldwell et al., 1998; Young and Phelps, 2005*]. Lacustrine sediment trap studies over the upper 100 m of the water column have found that degradation rate varies by chain length depending on sediment matrix and community composition in bottom waters [*Meyers et al.,* 1984; *Meyers and Eadie,* 1993].

In sediments, Canuel and Martens [1996] found that the greatest rate of degradation occurred in mid-chain length *n*-alkanes (C_{23}-C_{27}), while short (C_{17}-C_{21}) and long chain *n*-alkanes (>C_{25}) had slower degradation rates. In contrast, Lofthus et al. [2018] found that short chain *n*-alkanes (C_{13}-C_{15}) had the highest degradation rates and that long chain *n*-alkane degradation (C_{26}-C_{36}) rates varied in water temperatures between 5-10˚C. Indeed, many studies of microbial facilitated *n*-alkane degradation have shown substrate preferences for either short or long chain *n*-alkanes depending on the species present in the sediment [*Whyte et al.,* 1998; *So et al.,* 1999; *Bihari et al.,* 2010; *Liu et al.,* 2014].

Due to the uncertainty in *n*-alkane degradation by chain length and the lack of a site-specific study, we used other proxies to consider potential degradation impacts on our results. First, we examined the CPI with increasing depth (time) in the core. A lower CPI is typically indicative of greater degradation. No trend in the CPI with increasing core depth is observed (R^2 < 0.001), as the source of fresh OM input dominates the *n*-alkane signal (Supplemental Figure 1). We further found only trace amounts of phytane and pristine, degradation products of chlorophyll, and there were no trends in their concentrations with depth. Therefore, *n*-alkane degradation with increasing depth in the core is assumed to be minimal.

The relative distributions of *n*-alkanes may be further altered by secondary processes, such as production of odd chain *n*-alkanes by microbes in sediments. *Li et al*. [2018] specifically measured anaerobic microbe production of alkanes in peat and found that microbes produced a negligible amount of long and mid-chain *n*-alkanes. However, these anaerobic microbes did produce the short chain alkane, C_{19}, at a rate of 0.5% per year. Here, C_{19} production by microbes was assumed to be negligible since very few of our samples contained C_{19}. Samples that did contain C_{19} showed no trend in concentration with depth (R^2 = 0.04; Supplemental Figure 2). Thus, there is no evidence that secondary processing by microbial activity influences our results.

One final issue to consider is the limitation of source attribution of *n*-alkanes based on chain-length alone. Historically, long chain *n*-alkanes have been primarily attributed to terrestrial material. However, terrestrial sources may also produce a small amount of short chain *n*-alkanes

679 [*Kuhn et al*., 2010]. Similarly, algal sources have been found to produce some long chain alkanes
680 [*Lichtfouse et al*., 1994]. As such, samples with mixed *n*-alkane signatures may under- or over-
681 estimate a specific source. Other measurements in this study (e.g., trace elements, $\delta^{13}C$, $\delta^{15}N$),
682 however, confirm similarly high proportions of terrestrially derived material. Stable isotope
683 ($\delta^{13}C$ and $\delta^{15}N$) signatures during flood events are 2 and 4‰ lower, respectively, than
684 background, turbidite, and drought sediments, and are consistent with terrestrial OM values
685 [*Sweeney and Kaplan*, 1980; *Meyers*, 1994]. Additionally, SXRF data shows significantly higher
686 concentrations of lithogenic elements [*Hendy et al*., 2015]. Combined, these results confirm the
687 utility of the *n*-alkanes in characterizing source material in these sediments.
688
689 *4.5 Flood and Turbidite Sediment Contributions to Organic Carbon Burial*
690 In order to link modern processes with those observed in the sedimentary record, we
691 examined sediment trap material associated with 1997-98 El Niño flooding. The 1997-98 El
692 Niño was one of the wettest years on record with 202 mm of rainfall and an eight-fold increase in
693 lithogenic sedimentation rates in SBB [*Ross et al*., 1998; *Lange et al*., 2000; *Thunell*, 2003]. The
694 1997-98 El Niño sediment trap material is characterized by lower isotopic values and higher
695 terrestrial *n*-alkane concentrations relative to the background sediment trap, consistent with the
696 increase in terrestrial OM deposition. However, the El Niño sediment trap material contained no
697 macrophyte material, despite observations of kelp bed destruction during that time [*Lange et al*.,
698 2000]. Compared to the sediment core, the sediment traps have lower C/N ratios, consistent with
699 fresher sediment input, and isotopic ($\delta^{13}C$ and $\delta^{15}N$) signatures similar to background core
700 sediments. Furthermore, flood sediment trap terrestrial *n*-alkane concentrations are significantly
701 lower than those measured in the sediment core paleoflood events.
702 We hypothesize two mechanisms to explain the compositional differences between the
703 1997-98 El Niño sediment trap and flood layer sediments. First, the kelp rafts and flood plumes
704 bypassed the sediment trap; kelp rafts may have been too large to pass through the sediment trap
705 honeycomb, and flood plumes may have been transported downslope via gravity rather than
706 settling from the surface waters (See Section 4.2). Second, the processes that contribute to the
707 flood layers in SBB are significantly different than those associated with flooding during the
708 1997-98 El Niño.

Previous studies of SBB sediments have hypothesized the occurrence of megafloods; [*Schimmelmann et al.*, 1998; *Schimmelmann et al*., 2003; *Du et al*., 2018]; extreme floods associated with atmospheric rivers that produce massive amounts of precipitation and storm conditions [*Neiman et al*., 2008; *Dettinger et al*., 2011]. The most recent megaflood to occur in California was in 1861-1862 and is documented in the sediment core. The 1861-1862 megaflood, or "The Great Flood," occurred after ~ 40 days of continuous rain and historical reports of 25 inches that winter [*Newbold*, 1991; *Dettinger and Ingram*, 2013]. Megaflood layers in the sediment core occur every 166 ± 48 years in SBB, arguing that such events bury significant quantities of OC over a short time period. These 11 flood events are responsible for 15% of the TOC buried over the last 2,000 years. The largest flood event in the record (53 A.D.) may have accounted for 3% of the TOC buried alone. Furthermore, flood events are much more efficient in burying macrophyte and terrestrial derived OC, components that may have otherwise been remineralized in shallower oxygenated sediments if not transported and buried in the deeper ocean.

The 6 turbidites measured are responsible for remobilizing 12% of the total OC buried in the deep basin over the past 2,000 years. Although, turbidites also play a large role in C burial through high burial rates, this C was likely remobilized from the shelf. Turbidites therefore do not contribute to new C burial, but rather redistribute OC into low oxygen deep waters of the SBB where remineralization is likely to be slower [*Burdige*, 2006]. Non-event (background + drought) sediments are responsible for the bulk (75%) of the total OC buried, though at a much slower rate compared to flood or turbidite sediments. Regardless of the sedimentation process, the SBB buries a significant amount of OC from terrestrial and marine algal sources (Figure 7).

4.6 The Role of Terrestrial Organic Matter and Episodic Events in the Carbon Cycle

The burial of OC in oceanic sediments is a major sequestration pathway for carbon dioxide on geologic timescales with continental shelves representing the largest sink of both terrestrially and marine derived OC in the global ocean [*Berner*, 1982; *Martin et al*., 1987; *Sarmiento and Sundquist*, 1992; *Hedges and Keil*, 1995]. Indeed, estimates suggest that deltas and shelf sediments bury 30-35% of all of the terrestrially derived OC delivered by rivers globally [*Kandasamy and Nath*, 2016]. However, understanding OC sources, mechanisms of delivery, and burial along continental margins is complicated by their spatial and temporal

complexity, making predictions of the long term controls on the net drawdown of atmospheric carbon dioxide over past, modern day, and future regimes difficult to assess (e.g., *Bianchi et al*., 2018). One such hotspot of OC burial along the coast are small mountain river systems, such as those that deposit into the SBB, which may deliver as much as half of the world's global particulate OM to continental shelf systems [*Hatten et al*., 2010; *Bao et al*., 2015; *Hedges and Keil*, 1995]. This delivery may be highly episodic in nature as high relief and exposure to intense storm events result in turbid flow. Studies of continental margins have increasingly found that terrestrial OM is a much greater component of marine burial than previously realized (e.g., *Blair et al., 2004*; *Burdige et al*., 2005; *Bianchi et al.,* 2011). For example, in the Northern Gulf of Mexico, terrestrial OM accounted for 70-80% of OM burial [*Gordon and Goñi*, 2003] and off the coast of Washington, terrestrial OM comprised 10-30% of the sediment on the continental margin [*Keil et al*., 1994; *Prahl et al*., 1994].

Our study confirms these results; SBB sediments are comprised of substantial terrestrial OC. Although relatively infrequent, 11 flood events, comprising less than 1% of the total 2000 year record analyzed in this study, contribute 31% of all terrestrially derived OC buried. Terrestrial OM burial in marine sediments is an important climate feedback mechanism as the OC is often derived from vegetation and soil versus bedrock. Higher burial efficiencies relative to that on land coupled with this fresher non-rock derived OC results in marine terrestrial OM burial being an important sink of atmospheric CO_2 [*Stallard*, 1998]. Episodic floods occur worldwide (e.g., *Hilton et al*., 2008) and are likely to increase due to climate change [EASAC, 2018]. Western Europe in particular is susceptible to atmospheric river-induced floods [*Lavers and Villarini*, 2015], and areas surrounding the Pacific Ocean are susceptible to ENSO related flooding [*Muis et al*., 2018]. Our results highlight the complexity of the C cycle at the land-ocean interface and how episodic climate events may disproportionately impact C biogeochemistry. Incorporating these regions and episodic drivers of terrestrial OC burial into larger scale C cycle models is therefore critical for understanding past, present, and future C dynamics in light of increased flooding, sea level rise, and changes in land use.

5. Conclusions

Terrestrial OM is the dominant source of C buried in the SBB across all forms of deposition: flooding, turbidite remobilization, drought, and background conditions. Non-event

sedimentation in the SBB is responsible for 75% of the total OC buried over the last 2,000 years. Burial rates under these conditions are low (~0.43 g cm^{-2} kyr^{-1}) and OM sources include significant marine algal and macrophyte contributions. Droughts had a minimal impact on OC burial, however, they are composed of a larger proportion of marine material compared to the baseline. Episodic events (turbidites and floods) account for 25% of the OC buried, which is significant as these events occur over less than 1% of the time studied. While turbidites do not sequester new OC in SBB sediments, these events are responsible for the rapid remobilization of OC from the shelf to the deep basin. Turbidites contribute ~ 13% of the total OC buried in deep sea sediments over the past 2,000 years, with buried OC containing the highest concentrations of marine algal and macrophyte C relative to background, drought, and flood sedimentation.

Floods have the potential to bury significant amounts of OC in marine sediments through geologic time. In SBB, floods on the scale of megafloods are rare, occurring every 166 ± 48 years in the SBB, but have buried 11% of the TOC throughout the past 2,000 years. The main source of OC buried during these episodic flood events is terrestrially derived and is less degraded than terrestrial OC buried during background sedimentation. However, algae and macrophytes are still significant contributors to flood sediments. Increased algal concentrations in flood sediments is likely due to increased nutrient loads from river runoff and storm-driven mixing. Additionally, macrophyte deposition in floods sediments is likely associated with the destruction of kelp forests by waves during flood-associated storms. These results may be more widely relevant as episodic floods and turbidites, as well as drought intervals, are not limited to the Southern California region. Our results confirm that these processes may play a critical role in OC burial on continental margins around the world.

Acknowledgements

We would like to thank My (Phoebe) Le for her assistance processing samples. CBN, CD, CS and RT were supported by NSF OCE Grant: 1631977. IH was supported NSF OCE Grant 1304327. We thank Dorothy Pak for her assistance in the collection of kelp samples, Tiffany Napier for river bedload samples and Yi Wang for sampling SPR0901-03KC. Data will be provided as a supplemental file and will be available at **https://doi.org/10.1594/PANGAEA.917989**.

References

Altabet, M. A., Pilskaln, C., Thunell, R., Pride, C., Sigman, D., Chavez, F., & Francois, R. (1999). The nitrogen isotope biogeochemistry of sinking particles from the margin of the Eastern North Pacific. *Deep Sea Research Part I: Oceanographic Research Papers, 46*(4), 655-679. doi:10.1016/s0967-0637(98)00084-3

Bao, H., Lee, T., Huang, J., Feng, X., Dai, M., & Kao, S. (2015). Importance of Oceanian small mountainous rivers (SMRs) in global land-to-ocean output of lignin and modern biospheric carbon. *Scientific Reports, 5*(1). doi:10.1038/srep16217

Barron, J. A., Bukry, D., & Field, D. (2010). Santa Barbara Basin diatom and silicoflagellate response to global climate anomalies during the past 2200 years. *Quaternary International, 215*(1-2), 34-44. doi:10.1016/j.quaint.2008.08.007

Barron, J. A., Bukry, D., & Hendy, I. L. (2015). High-resolution paleoclimatology of the Santa Barbara Basin during the Medieval Climate Anomaly and early Little Ice Age based on diatom and silicoflagellate assemblages in Kasten core SPR0901-02KC. *Quaternary International, 387*, 13-22. doi:10.1016/j.quaint.2014.04.020

Berner, R. A. (1982). Burial of organic carbon and pyrite sulfur in the modern ocean; its geochemical and environmental significance. *American Journal of Science, 282*(4), 451-473. doi:10.2475/ajs.282.4.451

Bianchi, T. S. (2011). The role of terrestrially derived organic carbon in the coastal ocean: A changing paradigm and the priming effect. *Proceedings of the National Academy of Sciences, 108*(49), 19473-19481. doi:10.1073/pnas.1017982108

Bianchi, T. S., Cui, X., Blair, N. E., Burdige, D. J., Eglinton, T. I., & Galy, V. (2018). Centers of organic carbon burial and oxidation at the land-ocean interface. *Organic Geochemistry*, *115*, 138–155. doi: 10.1016/j.orggeochem.2017.09.008

Bihari, Z., Szabó, Z., Szvetnik, A., Balázs, M., Bartos, P., Tolmacsov, P., … Kiss, I. (2010). Characterization of a Novel Long-Chain n-Alkane-Degrading Strain, Dietzia sp. E1. *Zeitschrift Für Naturforschung C, 65*(11-12), 693–700. doi: 10.1515/znc-2010-11-1210

Blair, N. E., Leithold, E. L., & Aller, R. C. (2004). From bedrock to burial: the evolution of particulate organic carbon across coupled watershed-continental margin systems. *Marine Chemistry*, *92*(1-4), 141–156. doi: 10.1016/j.marchem.2004.06.023

Blaauw, M. & Christen, J. A. (2011). Flexible paleoclimate age-depth models using an autoregressive gamma process. *Bayesian Analysis, 6*(3), 457-474. doi:10.1214/11-BA618. https://projecteuclid.org/euclid.ba/1339616472

Blumer, M., & Clark Jr, R. C. (1967). DISTRIBUTION OF n-PARAFFINS IN MARINE ORGANISMS AND SEDIMENT. *Limnology and Oceanography, 12*(1), 79-87. doi:10.4319/lo.1967.12.1.0079

Bograd, S. J., & Lynn, R. J. (2001). Physical-biological coupling in the California Current during the 1997-99 El Niño-La Niña Cycle. *Geophysical Research Letters, 28*(2), 275-278. doi:10.1029/2000gl012047

Bograd, S. J., Schwing, F. B., Castro, C. G., & Timothy, D. A. (2002). Bottom water renewal in the Santa Barbara Basin. *Journal of Geophysical Research: Oceans, 107*(C12). doi:10.1029/2001jc001291

Brandes, J. A., Devol Allan, H., Yoshinari, T., Jayakumar, D. A., and Naqvi, S. W. A. (2003). Isotopic composition of nitrate in the central Arabian Sea and eastern tropical North Pacific: A tracer for mixing and nitrogen cycles. *Limnology and Oceanography, 43*(7), 1680-1689. doi: 10.4319/lo.1998.43.7.1680

Bray, E., & Evans, E. (1961). Distribution of n-paraffins as a clue to recognition of source beds. Geochimica Et Cosmochimica Acta, 22(1), 2-15. doi:10.1016/0016-7037(61)90069-2

Bray, N. A., Keyes, A., & Morawitz, W. M. (1999). The California Current system in the Southern California Bight and the Santa Barbara Channel. *Journal of Geophysical Research: Oceans, 104*(C4), 7695-7714. doi:10.1029/1998jc900038

Burdige, D. J. (2005). Burial of terrestrial organic matter in marine sediments: A re-assessment. *Global Biogeochemical Cycles, 19*(4). doi: 10.1029/2004gb002368

Burdige, D. J. (2006). *Geochemistry of marine sediments*. Princeton: Princeton University Press.

Caldwell, M. E., Garrett, R. M., Prince, R. C., & Suflita, J. M. (1998). Anaerobic Biodegradation of Long-Chainn-Alkanes under Sulfate-Reducing Conditions. *Environmental Science & Technology*, *32*(14), 2191–2195. doi: 10.1021/es9801083

Canuel, E. A., & Martens, C. S. (1996). Reactivity of recently deposited organic matter: Degradation of lipid compounds near the sediment-water interface. *Geochimica Et Cosmochimica Acta*, *60*(10), 1793–1806. doi: 10.1016/0016-7037(96)00045-2

Cavanaugh, K., Siegel, D., Reed, D., & Dennison, P. (2011). Environmental controls of giant-kelp biomass in the Santa Barbara Channel, California. *Marine Ecology Progress Series*, *429*, 1-17. doi:10.3354/meps09141

Chavez, F. P. (1996). Forcing and biological impact of onset of the 1992 El Nino in central California. *Geophysical Research Letters*, 23, 265-268.

Checkley, D. M., & Barth, J. A. (*2009*). Patterns and processes in the California Current System. *Progress in Oceanography*, *83*(1-4), 49–64. https://doi-org.proxy.lib.umich.edu/10.1016/j.pocean.2009.07.028

Cline, J., & Kaplan, I. (1975). Isotopic fractionation of dissolved nitrate during denitrification in the eastern tropical north pacific ocean. *Marine Chemistry*, *3*(4), 271-299. doi:10.1016/0304-4203(75)90009-2

Crisp, P., Brenner, S., Venkatesan, M., Ruth, E., & Kaplan, I. (1979). Organic chemical characterization of sediment-trap particulates from San Nicolas, Santa Barbara, Santa Monica and San Pedro Basins, California. *Geochimica Et Cosmochimica Acta*, *43*(11), 1791-1801. doi:10.1016/0016-7037(79)90027-9.

Davis, C.V., Ontiveros-Cuadras, J.F., Benitez-Nelson, C., Schmittner, A., Osborne, E., Tappa, E. & R.C. Thunell (2019). Ongoing increase in Eastern Tropical North Pacific denitrification as interpreted through sedimentary $\delta^{15}N$ from Santa Barbara Basin. *Paleoceanography and Paleoclimatology, this volume*

Dettinger, M. D., & Ingram, B. L. (2013). The Coming Megafloods. *Scientific American*, *308*(1), 64-71. doi:10.1038/scientificamerican0113-64

Dettinger, M. D., Ralph, F. M., Das, T., Neiman, P. J., & Cayan, D. R. (2011). Atmospheric Rivers, Floods and the Water Resources of California. *Water*, *3*(2), 445-478. doi:10.3390/w3020445

Deuser, W. G., Brewer, P. G., Jickells, T. D., & Commeau, R. F. (1983). Biological Control of the Removal of Abiogenic Particles from the Surface Ocean. *Science*, *219*(4583), 388-391. doi:10.1126/science.219.4583.388

Deutsch, C., Berelson, W., Thunell, R., Weber, T., Tems, C., McManus, J., Crusius, J., Ito, T., Baumgartner, T., Ferreira, V., Mey, J., Geen, A. V. (2014). Centennial changes in North Pacific anoxia linked to tropical trade winds. *Science, 345*(6197), 665-668. doi:10.1126/science.1252332

Dorman, C. E., & Winant, C. D. (2000). The Structure and Variability of the Marine Atmosphere around the Santa Barbara Channel. *Monthly Weather Review, 128*(2), 261. doi:10.1175/1520-0493(2000)1282.0.co;2

Du, X., Hendy, I., & Schimmelmann, A. (2018). A 9000-year flood history for Southern California: A revised stratigraphy of varved sediments in Santa Barbara Basin. *Marine Geology, 397*, 29-42. doi:10.1016/j.margeo.2017.11.014

EASAC. (2018). Extreme weather events in Europe. *European Academies Science Advisory Council*, 8 pp, https://easac.eu/fileadmin/PDF_s/reports_statements/Extreme_Weather/EASAC_Statement_Extreme_Weather_Events_March_2018_FINAL.pdf

Eglinton, G., Logan, G., Ambler, R., Boon, J., & Perizonius, W. (1991). Molecular Preservation [and Discussion]. *Philosophical Transactions: Biological Sciences, 333*(1268), 315-328.

Emery, K., & Hülsemann, J. (1962). The relationships of sediments, life and water in a marine basin. *Deep Sea Research, 8*(3-4). doi:10.1016/0146-6313(61)90019-3

Emmer, E., & Thunell, R. C. (2000). Nitrogen isotope variations in Santa Barbara Basin sediments: Implications for denitrification in the eastern tropical North Pacific during the last 50,000 years. *Paleoceanography, 15*(4), 377-387. doi:10.1029/1999pa000417

Ficken, K., Li, B., Swain, D., & Eglinton, G. (2000). An *n*-alkane proxy for the sedimentary input of submerged/floating freshwater aquatic macrophytes. *Organic Geochemistry, 31*(7-8), 745-749. doi:10.1016/s0146-6380(00)00081-4

Gordon, E. S., & Goñi, M. A. (2003). Sources and distribution of terrigenous organic matter delivered by the Atchafalaya River to sediments in the northern Gulf of Mexico. *Geochimica Et Cosmochimica Acta, 67*(13), 2359–2375. doi: 10.1016/s0016-7037(02)01412-6

Graham, N. E., Hughes, M. K., Ammann, C. M., Cobb, K. M., Hoerling, M. P., Kennett, D. J., ... Xu, T. (2007). Tropical Pacific – mid-latitude teleconnections in medieval times. *Climatic Change,83*(1-2), 241-285. doi:10.1007/s10584-007-9239-2

Grimalt, J., Albaiges, J., Al-Saad, H. T., & Douabul, A. A. (1985). *n*-Alkane distributions in surface sediments from the Arabian Gulf. *Naturwissenschaften, 72*(1), 35-37. doi:10.1007/bf00405327

Hatten, J. A., Goñi, M. A., & Wheatcroft, R. A. (2010). Chemical characteristics of particulate OM from a small, mountainous river system in the Oregon Coast Range, USA. *Biogeochemistry, 107*(1-3), 43-66. doi:10.1007/s10533-010-9529-z

Hedges, J., Clark, W., Quay, P., Richey, J., Devol, A., Santos, U. de M. (1986). Compositions and fluxes of particulate organic material in the Amazon River. *Limnology and Oceanography, 31*(4), 717—738. doi:10.4319/lo.1986.31.4.0717

Hedges, J. I., & Keil, R. G. (1995). Sedimentary OM preservation: An assessment and speculative synthesis. *Marine Chemistry, 49*(2-3), 81-115. doi:10.1016/0304-4203(95)00008-f

Hendy, I. L., Pedersen, T. F., Kennett, J. P., & Tada, R. (2004). Intermittent existence of a southern Californian upwelling cell during submillennial climate change of the last 60 kyr. *Paleoceanography, 19*(3). doi:10.1029/2003pa000965

Hendy, I. L., Dunn, L., Schimmelmann, A., & Pak, D. K. (2013). Resolving varve and radiocarbon chronology differences in the Santa Barbara basin sedimentary record, California. *Quaternary International, 387*, 155-168. doi:10.1016/j.quaint.2015.01.142

Hendy, I. L., Napier, T. J., & Schimmelmann, A. (2015). From extreme rainfall to drought: 250 years of annually resolved sediment deposition in Santa Barbara Basin, California. *Quaternary International, 387*, 3-12. doi:10.1016/j.quaint.2015.01.026

Heusser, L. E., Hendy, I. L., & Barron, J. A. (2015). Vegetation response to southern California drought during the Medieval Climate Anomaly and early Little Ice Age (AD 800–1600). *Quaternary International, 387*, 23-35. doi:10.1016/j.quaint.2014.09.032

Hilton, R. G., Galy, A., Hovius, N., Chen, M.-C., Horng, M.-J., & Chen, H. (2008). Tropical-cyclone-driven erosion of the terrestrial biosphere from mountains. *Nature Geoscience, 1*(11), 759–762. doi: 10.1038/ngeo333

Hülsemann, J., & Emery, K. O. (1961). Stratification in Recent Sediments of Santa Barbara Basin as Controlled by Organisms and Water Character. *The Journal of Geology, 69*(3), 279-290. doi:10.1086/626742

Kandasamy, S., & Nath, B. N. (2016). Perspectives on the Terrestrial Organic Matter Transport and Burial along the Land-Deep Sea Continuum: Caveats in Our Understanding of Biogeochemical Processes and Future Needs. *Frontiers in Marine Science*, *3*. doi: 10.3389/fmars.2016.00259

Keil, R. G., Montluçon, D. B., Prahl, F. G., & Hedges, J. I. (1994). Sorptive preservation of labile organic matter in marine sediments. *Nature*, *370*(6490), 549–552. doi: 10.1038/370549a0

Kuhn, T. K., Krull, E. S., Bowater, A., Grice, K., & Gleixner, G. (2010). The occurrence of short chain *n*-alkanes with an even over odd predominance in higher plants and soils. *Organic Geochemistry*, 41(2), 88–95. doi: 10.1016/j.orggeochem.2009.08.003

Lamontagne, M. G., Leifer, I., Bergmann, S., Werfhorst, L. C. V. D., & Holden, P. A. (2004). Bacterial diversity in marine hydrocarbon seep sediments. *Environmental Microbiology*, *6*(8), 799–808. doi: 10.1111/j.1462-2920.2004.00613.x

Lange, C. B., Weinheimer, A. L., Reid, F. M., Tappa, E., & Thunell, R. C. (2000). Response of siliceous microplankton from the Santa Barbara Basin to the 1997-98 El Niño event. *California Cooperative Oceanic Fisheries Reports*, *41*, 186-193.

Lavers, D. A. & Villarini, G. (2015). The contribution of atmospheric rivers to precipitation in Europe and the United States. *Journal of Hydrology*, *522*, 382-390, doi.org/10.1016/j.jhydrol.2014.12.010.

Li, C., Sessions, A. L., Kinnaman, F. S., & Valentine, D. L. (2009). Hydrogen-isotopic variability in lipids from Santa Barbara Basin sediments. *Geochimica Et Cosmochimica Acta*, *73*(16), 4803–4823. doi: 10.1016/j.gca.2009.05.056

Li, G., Li, L., Tarozo, R., Longo, W. M., Wang, K. J., Dong, H., & Huang, Y. (2018). Microbial production of long-chain n-alkanes: Implication for interpreting sedimentary leaf wax signals. *Organic Geochemistry*, *115*, 24–31. doi: 10.1016/j.orggeochem.2017.10.005

Lichtfouse, É., Derenne, S., Mariotti, A., & Largeau, C. (1994). Possible algal origin of long chain odd n-alkanes in immature sediments as revealed by distributions and carbon isotope ratios. *Organic Geochemistry*, *22*(6), 1023–1027. doi: 10.1016/0146-6380(94)90035-3

Liu, H., Xu, J., Liang, R., & Liu, J. (2014). Characterization of the Medium- and Long-Chain n-Alkanes Degrading Pseudomonas aeruginosa Strain SJTD-1 and Its Alkane Hydroxylase Genes. *PLoS ONE*, *9*(8). doi: 10.1371/journal.pone.0105506

Lofthus, S., Netzer, R., Lewin, A. S., Heggeset, T. M. B., Haugen, T., & Brakstad, O. G. (2018). Biodegradation of n-alkanes on oil–seawater interfaces at different temperatures and microbial communities associated with the degradation. *Biodegradation*, *29*(2), 141–157. doi: 10.1007/s10532-018-9819-z

Martin, J. H., Knauer, G. A., Karl, D. M., & Broenkow, W. W. (1987). VERTEX [Vertical Transport and Exchange]: Carbon cycling in the northeast Pacific. *Deep Sea Research Part B. Oceanographic Literature Review, 34*(9), 753. doi:10.1016/0198-0254(87)90148-8

Masiello, C. A., & Druffel, E. R. (2001). Carbon isotope geochemistry of the Santa Clara River. *Global Biogeochemical Cycles, 15*(2), 407-416. doi:10.1029/2000gb001290

Meyers, P. A. (1994). Preservation of elemental and isotopic source identification of sedimentary OM. *Chemical Geology, 114*(3-4), 289-302. doi:10.1016/0009- 2541(94)90059-0

Meyers, P. A. (2003). Applications of organic geochemistry to paleolimnological reconstructions: a summary of examples from the Laurentian Great Lakes. *Organic Geochemistry, 34*(2), 261-289. doi:10.1016/s0146-6380(02)00168-7

Meyers, P. A., & Eadie, B. J. (1993). Sources, degradation and recycling of organic matter associated with sinking particles in Lake Michigan. *Organic Geochemistry*, *20*(1), 47–56. doi: 10.1016/0146-6380(93)90080-u

Meyers, P. A., & Ishiwatari, R. (1993). Lacustrine organic geochemistry—an overview of indicators of organic matter sources and diagenesis in lake sediments. *Organic Geochemistry*, *20*(7), 867–900. doi: 10.1016/0146-6380(93)90100-p

Meyers, P., Leenheer, M., Eadie, B., & Maule, S. (1984). Organic geochemistry of suspended and settling particulate matter in Lake Michigan. *Geochimica Et Cosmochimica Acta*, *48*(3), 443–452. doi: 10.1016/0016-7037(84)90273-4

Muis, S., Haigh, I. D., Guimarães Nobre, G., Aerts, J. C. J. H., & Ward, P. J. (2018). Influence of El Niño-Southern Oscillation on global coastal flooding. Earth's Future, 6, 1311– 1322. https://doi.org/10.1029/2018EF000909

Mulder, T., & Syvitski, J. P. (1995). Turbidity Currents Generated at River Mouths during Exceptional Discharges to the World Oceans. *The Journal of Geology, 103*(3), 285-299. doi:10.1086/629747

Muller-Karger, F. E., Varela, R., Thunell, R., Luerssen, R., Hu, C., & Walsh, J. J. (2005). The importance of continental margins in the global carbon cycle. *Geophysical research letters, 32*(1), 1-4. doi: 10.1029/2004GL021346

Napier, T.J., Hendy, I.L., Fahnestock, M.F., and Bryce, J.G. (2019). Provenance of Santa Barbara Basin, California detrital sediments deposited during extreme climate events, *GSA Bulletin.* doi: 10.1130/B32035.1

Neiman, P. J., Ralph, F. M., Wick, G. A., Lundquist, J. D., & Dettinger, M. D. (2008). Meteorological Characteristics and Overland Precipitation Impacts of Atmospheric Rivers Affecting the West Coast of North America Based on Eight Years of SSM/I Satellite Observations. *Journal of Hydrometeorology, 9*(1), 22-47. doi:10.1175/2007jhm855.1

Newbold, J. D. (1991). *Th.e Great California Flood of 1861-1862* (Vol. 5, New Series, pp. 1-12, Rep. No. 4) (R. W. Clottu & J. Gillespie, Eds.). Lodi, CA: San Joaquin Historical Society.

Ogston, A., & Sternberg, R. (1999). Sediment-transport events on the northern California continental shelf. *Marine Geology, 154*(1-4), 69-82. doi:10.1016/s0025-3227(98)00104-2

Otero, M. P. & Siegel, D.A. (2004). Spatial and temporal characteristics of sediment plumes and phytoplankton blooms in the Santa Barbara Channel. *Deep Sea Research Part II: Topical Studies in Oceanography, 51*(10–11), 1129-1149, https://doi.org/10.1016/j.dsr2.2004.04.004

Pearson, A., & Eglinton, T. (2000). The origin of n -alkanes in Santa Monica Basin surface sediment: A model based on compound-specific Δ 14 C and δ 13 C data. *Organic Geochemistry, 31*(11), 1103-1116. doi:10.1016/s0146-6380(00)00121-2

Prahl, F., Ertel, J., Goni, M., Sparrow, M., & Eversmeyer, B. (1994). Terrestrial organic carbon contributions to sediments on the Washington margin. *Geochimica Et Cosmochimica Acta, 58*(14), 3035–3048. doi: 10.1016/0016-7037(94)90177-5

Rack, F., & Merrill, R. (1995). Interhole Correlations at Site 893, Santa Barbara Basin: Construction of a 16,000-Year Composite Record Using Magnetic Susceptibility and Digital Color Imaging Data. *Proceedings of the Ocean Drilling Program, Scientific Results 146 Part 2*. doi:10.2973/odp.proc.sr.146-2.287.1995

Ransom, B., K. F. Shea, P. J. Burkett, R. H. Bennett, & R. Baerwald (1998). Comparison of

pelagic and nepheloid layer marine snow: Implications for carbon cycling. *Marine Geology, 150*, 39–50. doi: 10.1016/S0025-3227(98)00052-8

Reimer, P. J., Bard, E., Bayliss, A., Beck, J. W., Blackwell, P. G., Ramsey, C. B., … Plicht, J. V. D. (2013). IntCal13 and Marine13 Radiocarbon Age Calibration Curves 0–50,000 Years cal BP. *Radiocarbon, 55*(4), 1869–1887. doi: 10.2458/azu_js_rc.55.16947

Reimers, C. E., Lange, C. B., Tabak, M., & Bernhard, J. M. (1990). Seasonal spillover and varve formation in the Santa Barbara Basin, California. *Limnology and Oceanography, 35*(7), 1577-1585. doi:10.4319/lo.1990.35.7.1577

Ropelewski, C. F., & Halpert, M. S. (1989). Precipitation Patterns Associated with the High Index Phase of the Southern Oscillation. *Journal of Climate, 2*(3), 268-284. doi:10.1175/1520-0442(1989)0022.0.co;2

Ross, T., Lott, N., McCown, S., & Quinn, D. (1998). *The El Nino Winter of '97 - '98* (pp. 1-28, Rep. No. 98-02). Asheville, NC: National Climatic Data Center.

Sarmiento, J. L., & Sundquist, E. T. (1992). Revised budget for the oceanic uptake of anthropogenic carbon dioxide. *Nature, 356*(6370), 589-593. doi:10.1038/356589a0

Scalan, E., & Smith, J. (1970). An improved measure of the odd-even predominance in the normal alkanes of sediment extracts and petroleum. *Geochimica Et Cosmochimica Acta, 34*(5), 611-620. doi:10.1016/0016-7037(70)90019-0

Schimmelmann, A., Hendy, I. L., Dunn, L., Pak, D. K., & Lange, C. B. (2013). Revised ~2000-year chronostratigraphy of partially varved marine sediment in Santa Barbara Basin, California. *Gff, 135*(3-4), 258–264. doi: 10.1080/11035897.2013.773066

Schimmelmann, A., Lange, C. B., & Meggers, B. J. (2003). Palaeoclimatic and archaeological evidence for a 200-yr recurrence of floods and droughts linking California, Mesoamerica and South America over the past 2000 years. *The Holocene, 13*(5), 763-778. doi:10.1191/0959683603hl661rp

Schimmelmann, A., & Tegner, M. J. (1991). Historical oceanographic events reflected in13C/12C ratio of total organic carbon in laminated Santa Barbara Basin Sediment. *Global Biogeochemical Cycles, 5*(2), 173-188. doi:10.1029/91gb00382

Schimmelmann, A., Zhao, M., Harvey, C. C., & Lange, C. B. (1998). A Large California Flood and Correlative Global Climatic Events 400 Years Ago. *Quaternary Research, 49*(01), 51-61. doi:10.1006/qres.1997.1937

Schlesinger, M. E., & Jiang, X. (1991). Climatic responses to increasing greenhouse gases, *Eos Transactions AGU*, *72*(53), 593– 593, doi:10.1029/90EO00417.

Schwarz, J. R., Walker, J. D., & Colwell, R. R. (1974). Deep-Sea Bacteria: Growth and Utilization of Hydrocarbons at Ambient and In Situ Pressure. *Applied Microbiology*, *28*(6), 982–986. doi: 10.1128/aem.28.6.982-986.1974

Sigman, D. M., Robinson, R., Knapp, A. N., van Geen, A., McCorkle, D. C., Brandes, J. A., & Thunell, R. C. (2003). Distinguishing between water column and sedimentary denitrification in the Santa Barbara Basin using the stable isotopes of nitrate, *Geochemistry. Geophysics, and Geosystems*, 4, 1040, doi:10.1029/2002GC000384, 5.

Smith, S. V., & Hollibaugh, J. T. (1993), Coastal metabolism and the oceanic organic carbon balance, *Reviews of Geophysics*, *31*(1), 75– 89, doi:10.1029/92RG02584.

So, C. M., & Young, L. Y. (1999). Isolation and Characterization of a Sulfate-Reducing Bacterium That Anaerobically Degrades Alkanes. *Applied and Environmental Microbiology*, *65*(7), 2969–2976. doi: 10.1128/aem.65.7.2969-2976.1999

Soutar, A., & Crill, P. A. (1977). Sedimentation and climatic patterns in the Santa Barbara Basin during the 19th and 20th centuries. *Geological Society of America Bulletin, 88*(8), 1161. doi:10.1130/0016-7606(1977)88<1161:sacpit>2.0.co;2

Soutar, A., Kling, S. A., Crill, P. A., Duffrin, E., & Bruland, K. W. (1977). Monitoring the marine environment through sedimentation. *Nature, 266*(5598), 136-139. doi:10.1038/266136a0

Stallard, R. F. (1998). Terrestrial sedimentation and the carbon cycle: Coupling weathering and erosion to carbon burial. *Global Biogeochemical Cycles, 12*(2), 231-257, doi:10.1029/98GB00741.

Sweeney, R. E., & Kaplan, I. (1980). Natural abundances of ^{15}N as a source indicator for near-shore marine sedimentary and dissolved nitrogen. *Marine Chemistry, 9*(2), 81-94. doi:10.1016/0304-4203(80)90062-6

Tems, C. E., Berelson, W. M., & Prokopenko, M. G. (2015). Particulate δ15N in laminated marine sediments as a proxy for mixing between the California Undercurrent and the California Current: A proof of concept. *Geophysical Research Letters, 42*(2), 419-427. doi:10.1002/2014gl061993

Thornton, S. E. (1984). Basin model for hemipelagic sedimentation in a tectonically active

continental margin: Santa Barbara Basin, California Continental Borderland. *Geological Society, London, Special Publications 15*, 377-394. doi: 10.1144/GSL.SP.1984.015.01.25

Thornton, S. E. (1986). Origin of mass flow sedimentary structures in hemipelagic basin deposits: Santa Barbara Basin, California Borderland. *Geo-Marine Letters*, *6*(1), 15–19. doi: 10.1007/bf02311691

Thunell, R.C. (1998). Seasonal and annual variability in particle fluxes in the Gulf of California: A response to climate forcing. *Deep Sea Research Part I: Oceanographic Research Papers*, 45. 2059-2083. 10.1016/S0967-0637(98)00053-3.

Thunell, R. C. (2003). Distinguishing between water column and sedimentary denitrification in the Santa Barbara Basin using the stable isotopes of nitrate. *Geochemistry, Geophysics, Geosystems, 4*(5). doi:10.1029/2002gc000384

Thunell, R. C., Tappa, E., & Anderson, D. M. (1995). Sediment fluxes and varve formation in Santa Barbara Basin, offshore California. *Geology*, *23*(12), 1083. doi: 10.1130/0091-7613(1995)023<1083:SFAVFI>2.3.CO;2

Voss, M., Dippner, J. W., & Montoya, J. P. (2001). Nitrogen isotope patterns in the oxygen-deficient waters of the Eastern Tropical North Pacific Ocean. *Deep Sea Research Part I: Oceanographic Research Papers, 48* (8), 1905-1921. doi: 10.1016/S0967-0637(00)00110-2

Wakeham, S. G., Hedges, J. I., Lee, C., Peterson, M. L., & Hernes, P. J. (1997). Compositions and transport of lipid biomarkers through the water column and surficial sediments of the equatorial Pacific Ocean. *Deep Sea Research Part II: Topical Studies in Oceanography*, *44*(9-10), 2131–2162. doi: 10.1016/s0967-0645(97)00035-0

Waliser, D., & Guan, B. (2017). Extreme winds and precipitation during landfall of atmospheric rivers. *Nature Geoscience*, *10*(3), 179-183. doi:10.1038/ngeo2894

Wang, Y. Hendy, I.L., and Thunell, R. (2019). Local and remote forcing of denitrification in the Northeast Pacific for the last 2000 years. *Paleoceanography and Paleoclimatology*

Wang, B., Yang, J., Jiang, H., Zhang, G., & Dong, H. (2019). Chemical composition of n-alkanes and microbially mediated n-alkane degradation potential differ in the sediments of Qinghai-Tibetan lakes with different salinity. *Chemical Geology*, *524*, 37–48. doi: 10.1016/j.chemgeo.2019.05.038

Warrick, J.A., DiGiacomo, P.M., Welsberg, S.B., Nezlin, N.P., Mengel, M., Jones,

B.H.,Ohlmann, J. C., Washburn, L., Terrill, E. J., & Farnsworth, K. L. (2007). River plume patterns and dynamics within the Southern California Bight. *Continental Shelf Research, 27*(19), 2427-2448. doi: 10.1016/j.csr.2007.06.015

Warrick, J. A., Washburn, L., Brzezinski, M. A., & Siegel, D. A. (2005). Nutrient contributions to the Santa Barbara Channel, California, from the ephemeral Santa Clara River. *Estuarine, Coastal and Shelf Science, 62*(4), 559-574. doi:10.1016/j.ecss.2004.09.033

Warrick, J.A., and Farnsworth, K.L. (2009). Sources of sediment to the coastal waters of the Southern California Bight, in Lee, H.J., & Normark, W.R., eds., Earth Science in the Urban Ocean: The Southern California Continental Borderland: Geological Society of America Special Paper 454, p. 39–52, doi: 10.1130/2009.2454(2.2)

Whyte, L. G., Hawari, J., Zhou, E., Bourbonnière Luc, Inniss, W. E., & Greer, C. W. (1998). Biodegradation of Variable-Chain-Length Alkanes at Low Temperatures by a Psychrotrophic Rhodococcussp. *Applied and Environmental Microbiology*, *64*(7), 2578–2584. doi: 10.1128/aem.64.7.2578-2584.1998

Wroblewski, J. S. & Richman, J. G. (1987) The non-linear response of plankton to wind mixing events - implications for survival of larval northern anchovy, *Journal of Plankton Research, 9*(1), 103–123, https://doi.org/10.1093/plankt/9.1.103

Young, L. Y., & Phelps, C. D. (2005). Metabolic Biomarkers for Monitoringin SituAnaerobic Hydrocarbon Degradation. *Environmental Health Perspectives, 113*(1), 62–67. doi: 10.1289/ehp.6940

Figure 1: Map of the Santa Barbara Basin (SBB). The sediment core is labeled by the red square (34°16.99’N, 120°2.41’W), the sediment trap is denoted by the yellow triangle (34°14′N, 120°02′W), and the river collection sites are marked by the purple circles (see *Napier et al.* [2019]): Santa Clara River, location 13 (34˚23.10’ N, 118˚47.22’W) and 16 (34˚20.70’N, 119˚01.46’W); Ventura River, location 21 (34˚25.20’N, 119˚ 17.94’W); and the Santa Ynez River, locations 22 (34˚24.60’N, 119˚49.74’W) and 30 (34˚38.40’N, 120˚24.54’W). Kelp beds are denoted by shaded orange regions in the nearshore environment of the SBB [*Schimmelmann and Tegner*, 1991].

Figure 2: Box plot comparisons of composition by sediment type: Flood (dark blue solid box), turbidites (pale gray diagonal striped box), background (dark green speckled box), and drought (orange horizontal striped box) sediments relative to sediment trap background (pale green dashed box) and flood (pale blue dashed horizontal striped box) for **A.** Total Organic Carbon (weight %), **B.** Total Nitrogen (weight %), **C.** C/N ratio, **D.** $\delta^{13}C$ (‰ SMOW) and **E.** $\delta^{15}N$ (‰). Within each box, the line is the median, the X is the mean, and points outside of the boxes (greater than 1.5 quartiles) are outliers.

Figure 3: Uncorrected depth profiles spanning the past 2,000 years from the SBB sediment record. **A.** Total Organic Carbon (TOC) Mass Accumulation Rates (MAR) (g, cm^{-2}, kyr^{-1}; black line), **B.** Molar C/N ratio (purple line), **C.** Total Nitrogen (TN) (weight %; blue line), **D.** Total Organic Carbon (TOC) (weight %; red line), and **E.** $\delta^{13}C$ (‰ SMOW; black crosses) and $\delta^{15}N$ (‰; green line) vary during instantaneous events, such as flooding (blue shaded bars), turbidites (tan shaded bars) [*Du et al*., 2018], and droughts (red shaded bars) [*Heusser et al*., 2015].

Figure 4: Comparison of 2,000 years of $\delta^{15}N$ (‰; green line) and *n*-alkane concentrations normalized to TOC (µg/g TOC) by depth in sediment core. The concentration of terrestrial (C_{27}, C_{29}, C_{31}, C_{33}; grey circles), macrophyte (C_{21}, C_{23}; white squares) and algal (C_{15}, C_{17}, C_{19}; black triangles) *n*-alkanes varies during instantaneous events such as flooding (blue bars), and turbidites (tan bars) [*Du et al*., 2018] as well as during droughts intervals (pink bars) [*Heusser et al*., 2015]. Note: *n*-alkane concentrations depicted as 0 are Below Detection Limit (BDL) of 0.5 mg/L in hexane on the GC/MS.

Figure 5: Box plot comparison of normalized concentrations (µg/g TOC) of *n*-alkane source by sediment type: Flood (dark blue solid box), turbidites (pale gray diagonal striped box), background (dark green speckled box), and drought (orange horizontal striped box) sediments relative to sediment trap background (pale green dashed box) and flood (pale blue dashed horizontal striped box) material for **A.** terrestrial (C_{27}, C_{29}, C_{31}, C_{33}), **B.** algal (C_{15}, C_{17}, C_{19}), and **C.** macrophyte (C_{21}, C_{23}) *n*-alkanes. Within each box, the line is the median, the X is the mean, and points outside of the box are outliers.

Figure 6: The relative contribution of *n*-alkane sources in Santa Barbara Basin sediments: **A.** background sediments, **B.** drought intervals, **C.** flood events, and **D.** turbidites. Terrestrial *n*-alkanes (C_{27}, C_{29}, C_{31}, C_{33}; tan, speckled shading) dominate all sediment types. Macrophyte *n*-alkanes (C_{21}, C_{23}) are depicted by the dark green shading with diagonal lines, and algal *n*-alkanes (C_{15}, C_{17}, C_{19}) are depicted by the blue shading with horizontal lines.

1200

1201 **Figure 7:** The relative contribution of each sediment type to burial of Total Organic Carbon and different
1202 *n*-alkane sources in SBB sediments. Carbon burial is divided into: **A.** organic carbon, **B.** terrestrial (C_{27},
1203 C_{29}, C_{31}, C_{33}) carbon, **C.** macrophyte (C_{21}, C_{23}) carbon, and **D.** algal (C_{15}, C_{17}, C_{19}) carbon, where green
1204 speckled shading represents background sediments, tan horizontally striped shading represents drought
1205 intervals, dark blue shading represents flood events sediments and grey diagonal shading represents
1206 turbidites.

1207

Figure 1.

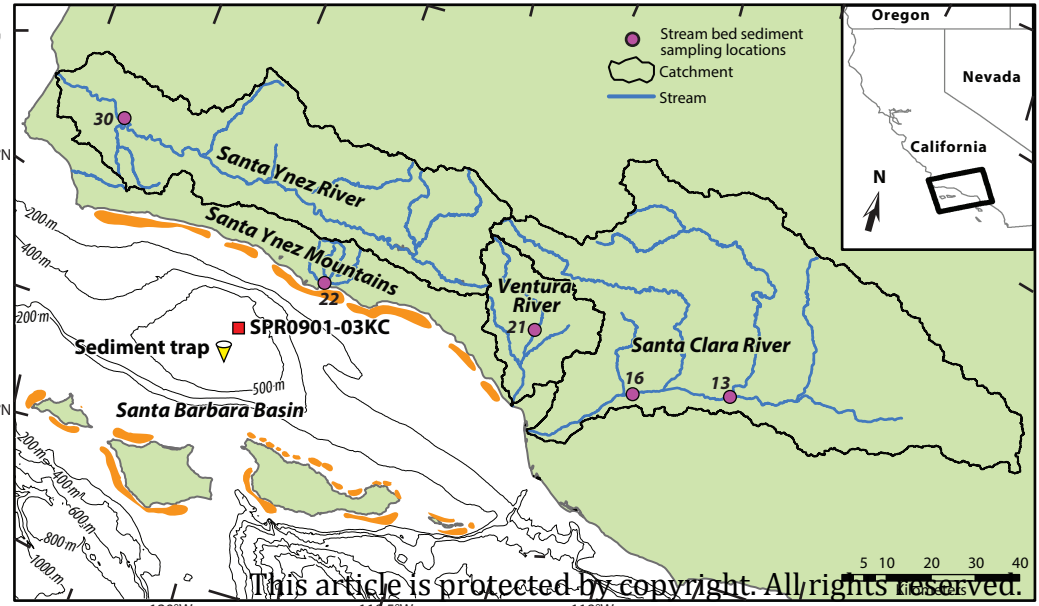

Figure 2.

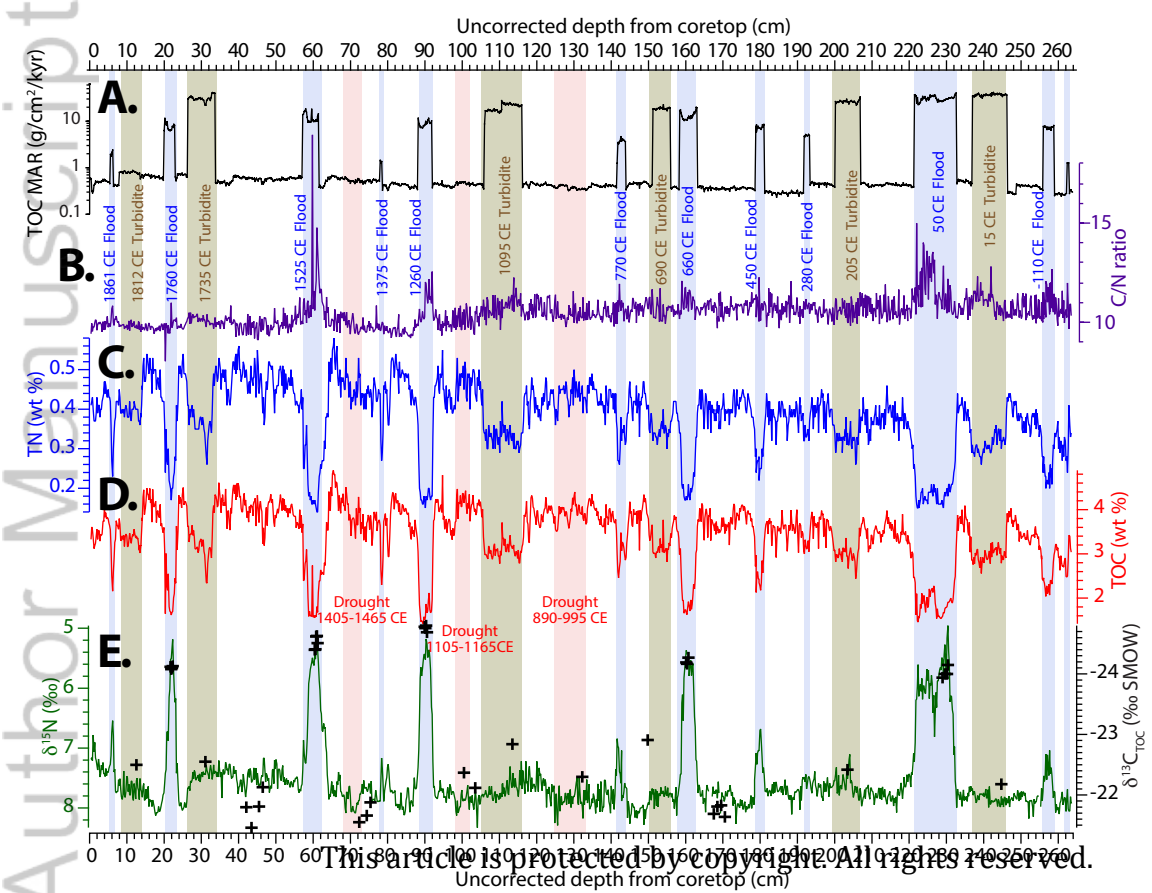

Figure 3.

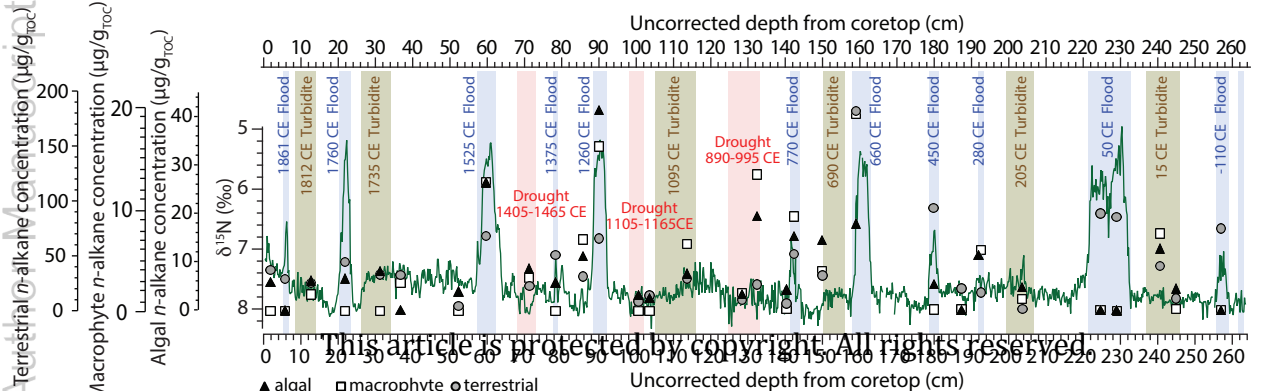

Figure 4.

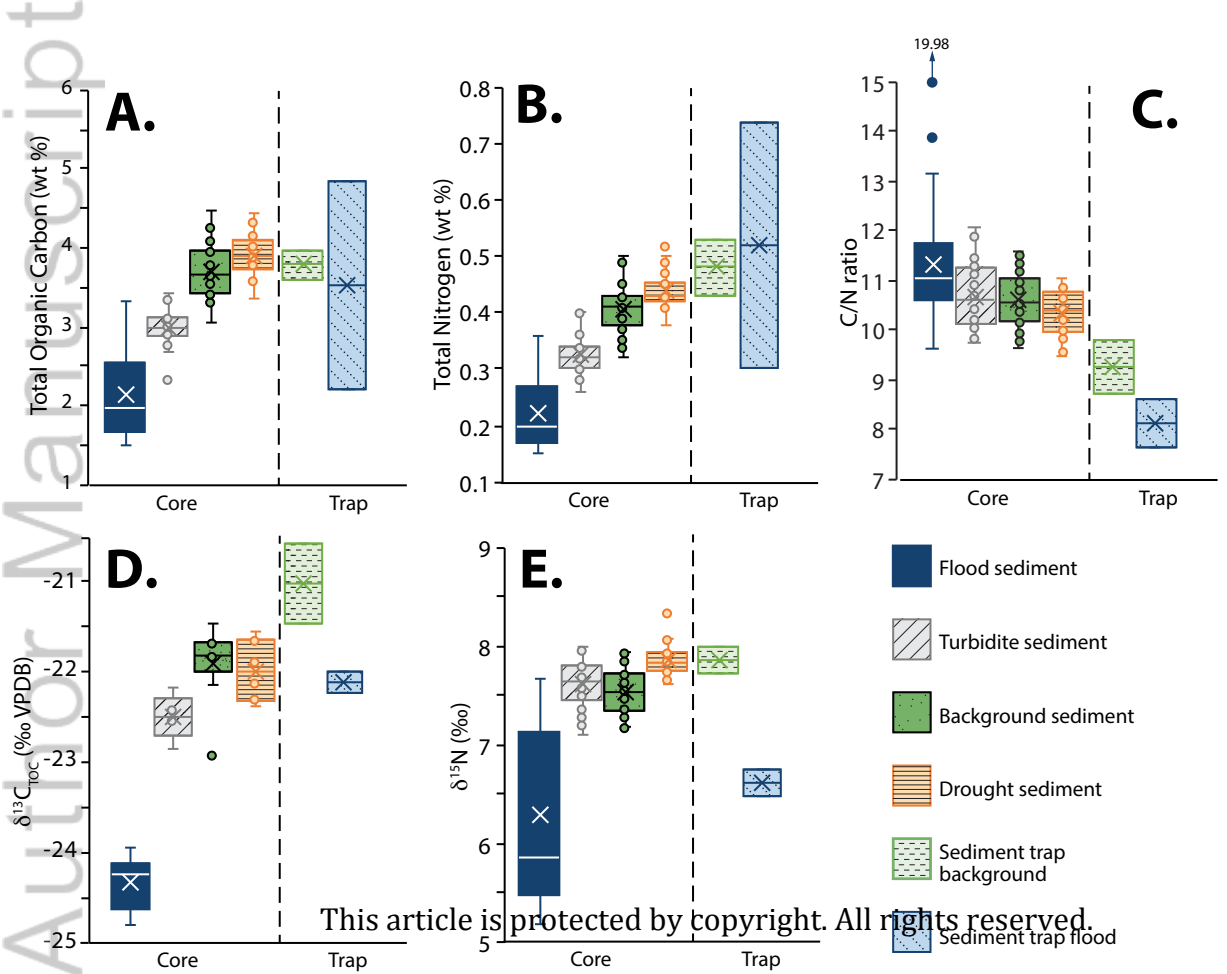

Figure 5.

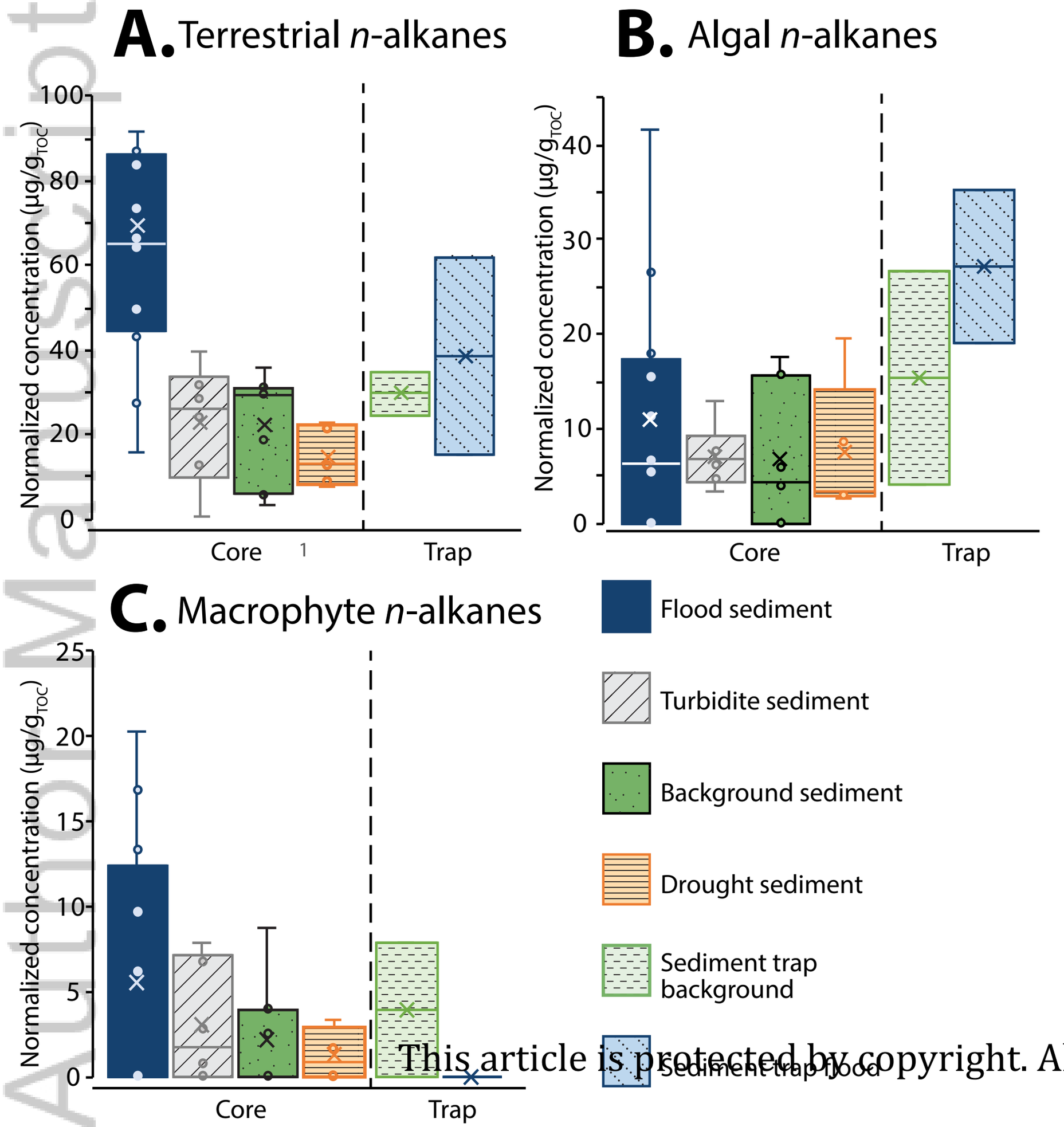

Figure 6.

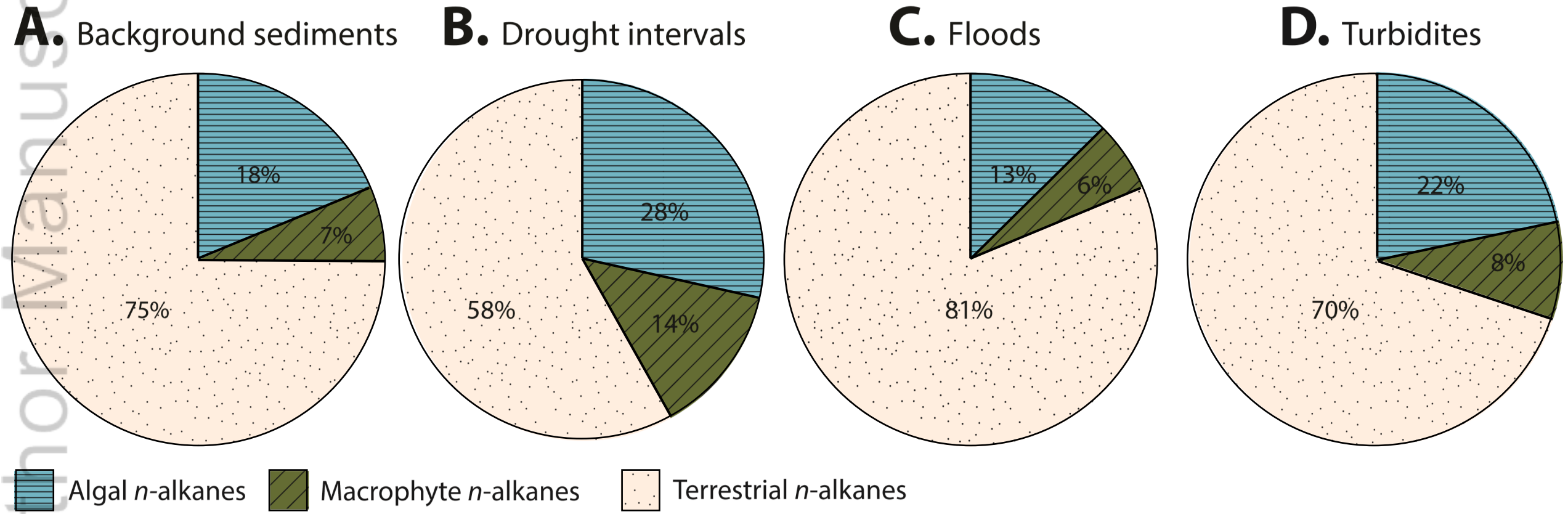

Figure 7.

Carbon Burial

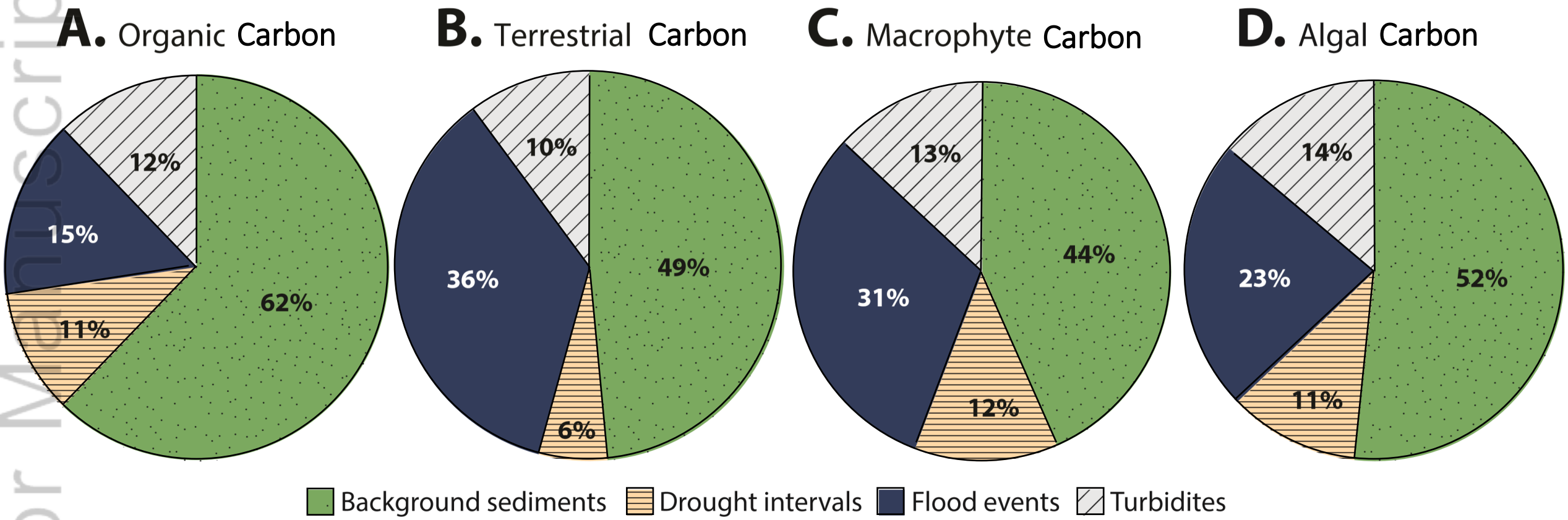

Table 1: Average relative abundance of Total Organic Carbon (TOC), and Total Nitrogen (TN) and molar C/N ratios and isotopic composition in Santa Barbara Basin sediments and sediment end members.

	Background	**Drought**	**Flood**	**Turbidite**	**Kelp**	**Sediment Trap Background**	**Sediment Trap Flood**
	n=33	*n=25*	*n=58*	*n=34*	*n=1*	*n=2*	*n=2*
TOC (wt %)	3.70 ± 0.31	3.90 ± 0.25	2.13 ± 0.53	2.98 ± 0.23	13.79	3.79 ± 0.25	3.53 ± 1.87
TN (wt %)	0.41 ± 0.04	0.44 ± 0.03	0.22 ± 0.06	0.33 ± 0.03	1.04	0.48 ± 0.07	0.52 ± 0.31
C/N	10.67 ± 0.47	10.34 ± 0.28	11.45 ± 1.03	10.63 ± 0.55	15.47	9.27 ± 0.75	8.12 ± 0.67
$\delta^{13}C$ (‰)	-21.9 ± 0.09	-21.98 ± 0.09	-24.34 ± 0.84	-22.5 ± 0.21	-14.73	-21.01 ± 0.64	-22.12 ± 0.16
$\delta^{15}N$ (‰)	7.54 ± 0.20	7.88 ± 0.09	6.26 ± 0.84	7.59 ± 0.21	9.79	7.87 ± 0.19	6.62 ± 0.21

Table 2: Relative concentrations of Total Organic Carbon (TOC), Total Nitrogen (TN), *n*-alkanes, C/N ratios and isotopic composition of bed load sediments in rivers draining into the Santa Barbara Basin.

Location Number*	**13** **Santa Clara River**	**16** **Santa Clara River**	**21** **Ventura River**	**22** **Santa Ynez River**	**30** **Santa Ynez River**	**Average** **River Sediment**
Latitude, Longitude	34°23.10'N, 118°47.22'W	34°20.70'N, 119°01.46'W	34°25.20'N, 119°17.94'W	34°24.60'N, 119°49.74'W	34°38.40'N, 120°24.54'W	--
C_{25} (µg/gOC)	6	BDL	BDL	7	12	5 ± 5
Terrestrial C_{27}, C_{29}, C_{31} (µg/gOC)	147	146	820	118	192	285 ± 269
TOC	2.68	0.43	0.87	2.13	1.15	1.45 ± 0.93
TN	0.25	0.07	0.12	0.19	0.14	0.15 ± 0.07
C/N	12.51	7.17	8.46	13.08	9.58	10.16 ± 2.56
$\delta^{13}C$ (‰)	-24.77	-31.53	-22.80	-27.10	-24.05	-26.05 ± 3.44
$\delta^{15}N$ (‰)	7.00	8.51	4.41	6.28	6.30	6.50 ± 1.48

* Samples location description in *Napier et al*., 2019

Table 3: Concentration of *n*-alkanes in Santa Barbara Basin sediments and end members.

	Background *n=7*	**Flood** *n=12*	**Turbidite** *n=6*	**Drought** *n=5*	**Kelp** *n=1*	**Sediment Trap Baseline** *n=2*	**Sediment Trap Flood** *n=2*	**Rivers** *n=5*
CPI	2.41 ±1.90	3.47 ± 1.67	4.08 ± 4.79	2.78 ± 2.45	2.12	5.96 ± 2.34	3.33 ± 1.12	Only Odds
Algal C_{15}, C_{17}, C_{19} (µg/gOC)	6 ± 5	11 ± 13	7 ± 3	7 ± 7	16	20 ± 22	27 ± 11	BDL
Macrophyte C_{21}, C_{23} (µg/gOC)	2 ± 3	5 ± 7	3 ± 3	4 ± 6	7	5 ± 7	BDL	BDL
Terrestrial C_{27}, C_{29}, C_{31} (µg/gOC)	23 ± 13	70 ± 42	23 ± 14	15 ± 7	BDL	30 ± 7	40 ± 33	285 ± 300

Table 4: Sedimentation and burial rates in Santa Barbara Basin sediments.

		Sedimentation Rate (mm, yr^{-1})	Mass Accumulation Rate (g, cm^{-2}, yr^{-1})	OC Burial Rate (g, cm^{-2}, kyr^{-1})	Terrestrial Burial Rate (µg, cm^{-2}, kyr^{-1})	Macrophyte Burial Rate (µg, cm^{-2}, kyr^{-1})	Algal Burial Rate (µg, cm^{-2}, kyr^{-1})
Background	*n = 7*	0.95 ± 0.19	0.0236 ± 0.04	0.43 ± 0.09	9.61 ± 6.27	0.84 ± 1.22	2.43 ± 0.10
Drought	*n = 5*	0.85 ± 0.14	0.0107 ± 0.002	0.42 ± 0.07	6.41 ± 3.27	1.35 ± 1.93	2.99 ± 2.54
Flood	*n = 12*	38.30 ± 34*	0.6205 ± 0.51	11.52 ± 8.9	439 ± 612	37.3 ± 74.4	67.6 ± 112
Turbidite	*n = 6*	61.74 ± 32*	0.8359 ± 0.45	24.37 ± 12.4	578 ± 548	72.2 ± 111.8	188 ± 155

* Assuming each instantaneous event has a duration of one year.

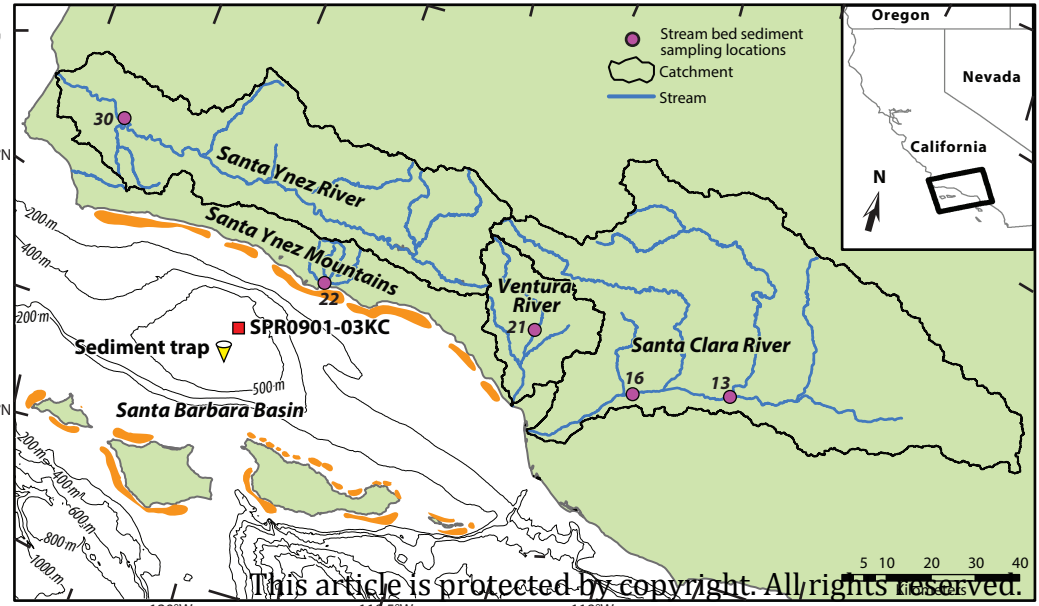

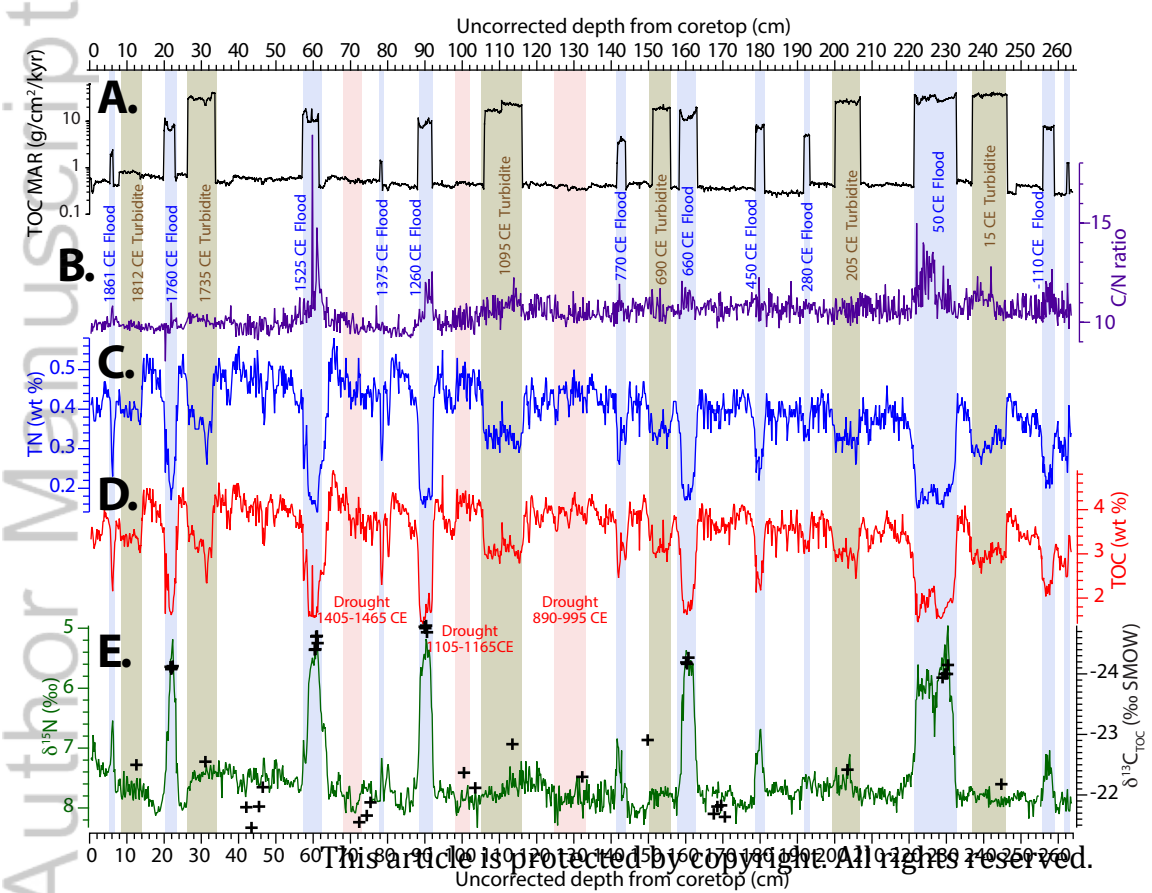

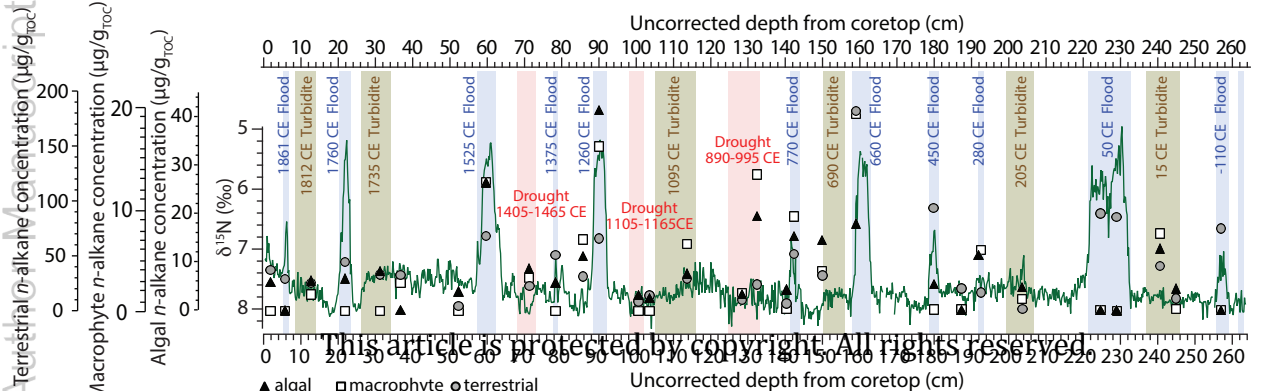

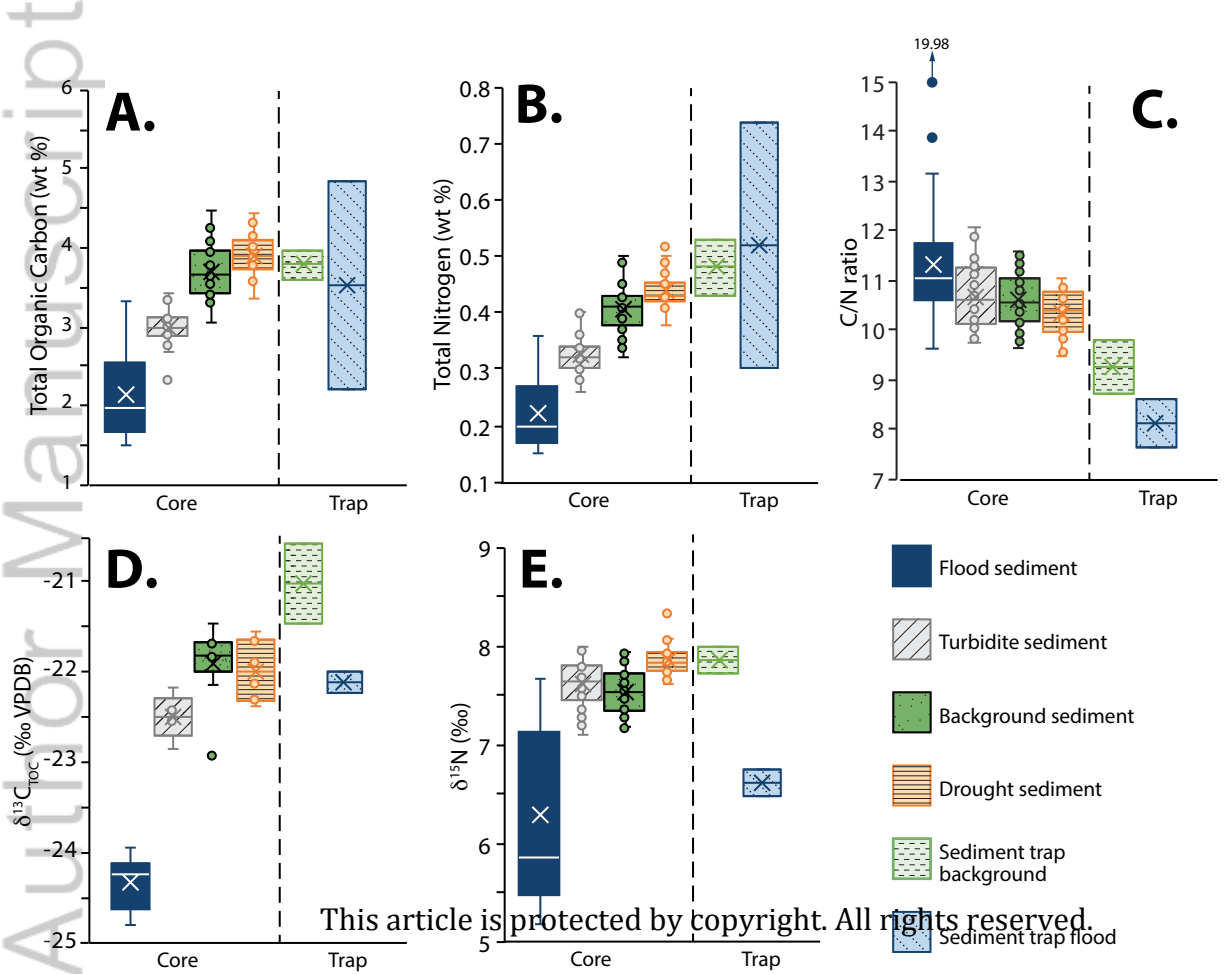

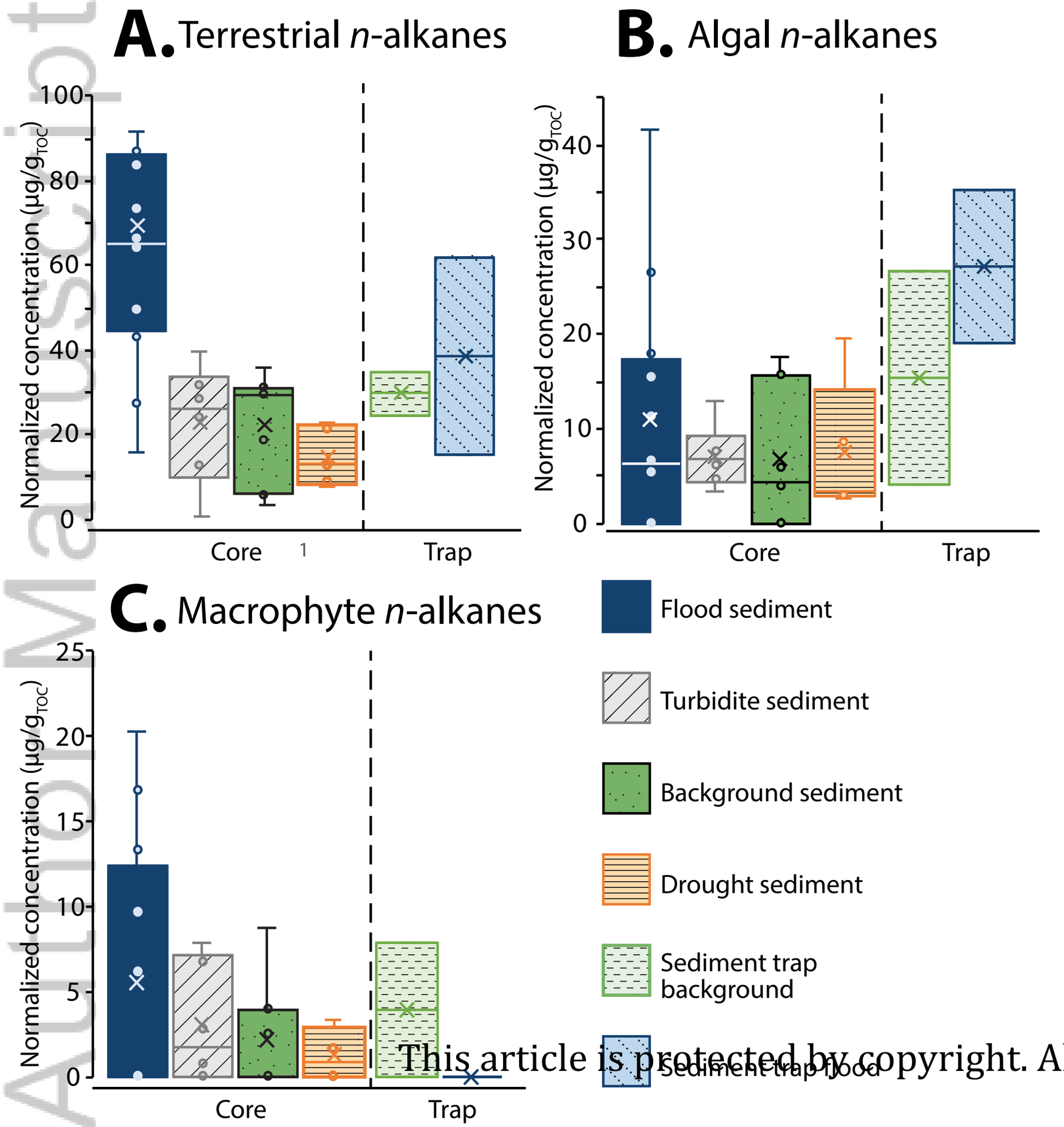

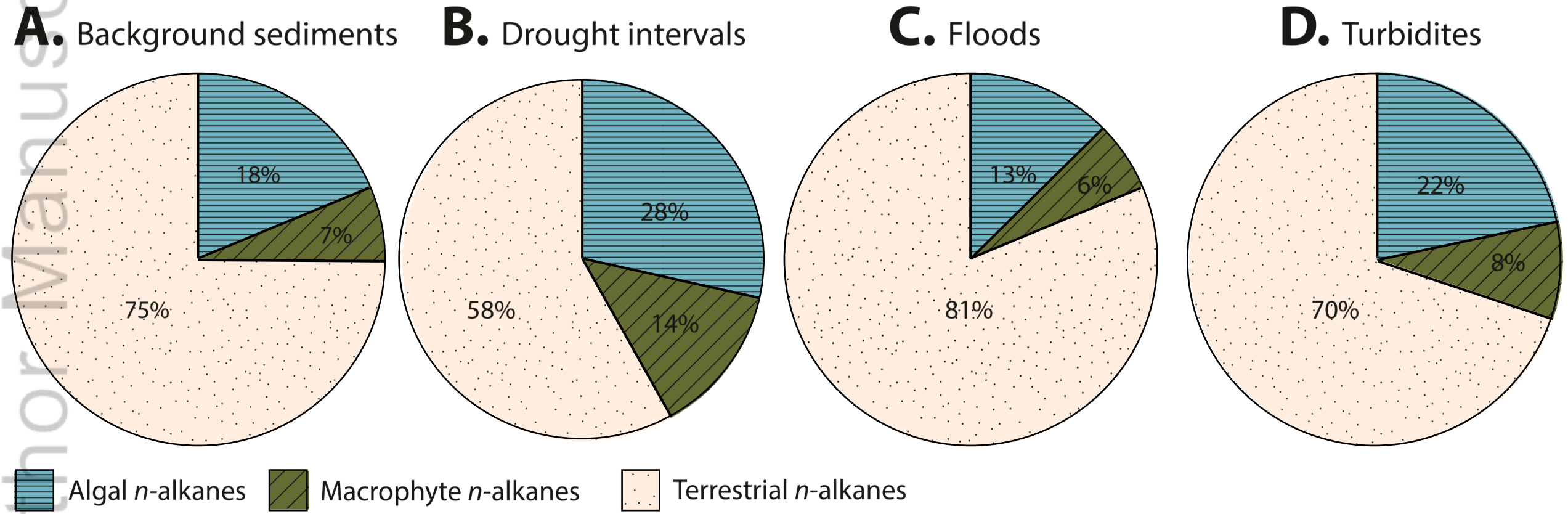

Carbon Burial